Am J Physiol Heart Circ Physiol 317: H445–H459, 2019.
First published June 7, 2019; doi:10.1152/ajpheart.00738.2018.

RESEARCH ARTICLE | *Integrative Cardiovascular Physiology and Pathophysiology*

Chronic intermittent electronic cigarette exposure induces cardiac dysfunction and atherosclerosis in apolipoprotein-E knockout mice

Jorge Espinoza-Derout,[1] Kamrul M. Hasan,[1] Xuesi M. Shao,[1,2] Maria C. Jordan,[2] Carl Sims,[1] Desean L. Lee,[1] Satyesh Sinha,[1,2] Zena Simmons,[1] Norma Mtume,[1] Yanjun Liu,[1,2] Kenneth P. Roos,[2] Amiya P. Sinha-Hikim,[1,2] and Theodore C. Friedman[1,2]

[1]*Division of Endocrinology, Metabolism and Molecular Medicine, Department of Internal Medicine, Charles R. Drew University of Medicine and Science, Los Angeles, California; and* [2]*David Geffen School of Medicine at University of California, Los Angeles, California*

Submitted 16 November 2018; accepted in final form 28 May 2019

Espinoza-Derout J, Hasan KM, Shao XM, Jordan MC, Sims C, Lee DL, Sinha S, Simmons Z, Mtume N, Liu Y, Roos KP, Sinha-Hikim AP, Friedman TC. Chronic intermittent electronic cigarette exposure induces cardiac dysfunction and atherosclerosis in apolipoprotein-E knockout mice. *Am J Physiol Heart Circ Physiol* 317: H445–H459, 2019. First published June 7, 2019; doi:10.1152/ajpheart.00738.2018.—Electronic cigarettes (e-cigarettes), also known as electronic nicotine delivery systems, are a popular alternative to conventional nicotine cigarettes, both among smokers and those who have never smoked. In spite of the widespread use of e-cigarettes and the proposed detrimental cardiac and atherosclerotic effects of nicotine, the effects of e-cigarettes on these systems are not known. In this study, we investigated the cardiovascular and cardiac effects of e-cigarettes with and without nicotine in apolipoprotein-E knockout ($ApoE^{-/-}$) mice. We developed an e-cigarette exposure model that delivers nicotine in a manner similar to that of human e-cigarettes users. Using commercially available e-cigarettes, bluCig PLUS, $ApoE^{-/-}$ mice were exposed to saline, e-cigarette without nicotine [e-cigarette (0%)], and e-cigarette with 2.4% nicotine [e-cigarette (2.4%)] aerosol for 12 wk. Echocardiographic data show that mice treated with e-cigarette (2.4%) had decreased left ventricular fractional shortening and ejection fraction compared with e-cigarette (0%) and saline. Ventricular transcriptomic analysis revealed changes in genes associated with metabolism, circadian rhythm, and inflammation in e-cigarette (2.4%)-treated $ApoE^{-/-}$ mice. Transmission electron microscopy revealed that cardiomyocytes of mice treated with e-cigarette (2.4%) exhibited ultrastructural abnormalities indicative of cardiomyopathy. Additionally, we observed increased oxidative stress and mitochondrial DNA mutations in mice treated with e-cigarette (2.4%). $ApoE^{-/-}$ mice on e-cigarette (2.4%) had also increased atherosclerotic lesions compared with saline aerosol-treated mice. These results demonstrate adverse effects of e-cigarettes on cardiac function in mice.

NEW & NOTEWORTHY The present study is the first to show that mice exposed to nicotine electronic cigarettes (e-cigarettes) have decreased cardiac fractional shortening and ejection fraction in comparison with controls. RNA-seq analysis reveals a proinflammatory phenotype induced by e-cigarettes with nicotine. We also found increased atherosclerosis in the aortic root of mice treated with e-cigarettes with nicotine. Our results show that e-cigarettes with nicotine lead to detrimental effects on the heart that should serve as a warning to e-cigarette users and agencies that regulate them.

Address for reprint requests and other correspondence: J. Espinoza-Derout, Charles R. Drew Univ. of Medicine and Science, 1731 E. 120th St. LSRNE Bldg.-Rm. N220, Los Angeles, CA 90059 (e-mail: jorgeespinozaderout@cdrewu.edu).

atherosclerosis; cardiomyopathy; cardiovascular disease; inflammation; myocardial biology

INTRODUCTION

Without combusting tobacco, electronic cigarettes (e-cigarettes, also called electronic nicotine delivery systems) are becoming a popular world-wide alternative to conventional tobacco cigarettes, both in smokers and people who have never smoked (60). Among United States adolescents, e-cigarettes are the most frequently used tobacco product (41). Additionally, in the belief that e-cigarettes are harmless, people addicted to nicotine use e-cigarettes as a way to avoid combustion-generated toxicants or to aid in smoking cessation (8). E-cigarettes are battery-powered devices resembling a cigarette that contains a circuit activated by drawing on the mouthpiece (78). A recent study found that e-cigarettes help with decreasing the use of combustible cigarettes (30), although a review article suggested that they may increase smoking rates by appealing to young consumers (27). Therefore, there is an urgent need for a better understanding of the health effects, including cardiovascular effects, of e-cigarette use to inform regulatory agencies, medical practitioners, and the general public.

Conventional cigarettes affect two distinct cardiac processes (8): *1*) heart failure, which is characterized by decreased cardiac output, and *2*) atherosclerosis or coronary artery disease, in which atherosclerotic lesions build up in coronary arteries, leading to blockage of one or more coronary arteries that results in myocardial infarction. Smoking is an independent risk factor for heart failure (8). In rodent models, nicotine can trigger cardiomyocyte (CM) apoptosis (75). In spite of the widespread use of e-cigarettes and the detrimental cardiac and cardiovascular effects of nicotine, systematic evaluation of the chronic effects of e-cigarettes on these outcomes is lacking. Epidemiological cross-sectional studies have shown an independent association with increased odds of myocardial infarction in e-cigarette users (3). Although there is experimental evidence that nicotine contributes to accelerating atherosclerosis and cardiovascular changes (80), these effects do not take into consideration of the different delivery systems of e-cigarettes. Also, these studies do not examine the unknown cardiovascular effects of substances present in e-cigarettes but absent in conventional cigarettes, such as aldehydes, propylene gly-

col/glycerol particulates, and flavors as well as the atomizer system in which e-cigarettes are heated to a high temperature (9). Therefore, it is crucial to test the effects of e-cigarettes on the cardiovascular system in animal models using a vaping-relevant delivery system.

Several interacting pathways have a role in the nicotine's effects on cardiovascular damage, including exacerbation of oxidative stress, chronic inflammation, and insulin resistance (12, 81). In adipocytes, nicotinic acetylcholine receptor subunit-α7 mediates nicotine-stimulated AMP-activated protein kinase activation that leads to release of free fatty acids (FFAs) (82). FFAs are one of the key elements in ectopic lipid accumulation, lipotoxicity, mitochondrial dysfunction (18, 33, 35), and cardiomyopathy (14, 17). FFAs can increase mitochondrial generation of reactive oxygen species (ROS), which have been implicated as a major mechanism of metabolic syndrome and cardiomyopathy (20, 71). Mitochondrial ROS generation contributes to the activation of maladaptive signaling, including leading to impaired calcium handling, a fundamental feature of most forms of systolic dysfunction and heart disease (51).

Apolipoprotein-E knockout ($ApoE^{-/-}$) mice, a widely used murine model of atherosclerosis (65), have been used to study the cardiovascular effects of conventional cigarettes (50). $ApoE^{-/-}$ mice share greater degrees of similarity in the atherosclerotic development with humans compared with wild-type models (25) that are resistant to cardiovascular inflammation and atherosclerosis (84). Wild-type C57Bl/6 mice have been exposed to e-cigarettes with nicotine for 8 mo without showing a significant change in fractional shortening or ejection fraction (63). Therefore, we used an $ApoE^{-/-}$ mouse model to study the effects of e-cigarettes with and without nicotine on cardiovascular function and pathophysiology as compared with wild-type C57BL/6J mice (63).

METHODS

Animals. Animal handling and experimentation were in accordance with the recommendation of the current National Institutes of Health guidelines and were approved by the Charles R. Drew University School of Medicine and Science Institutional Animal Care and Use Committee. Male C57BL/6J $ApoE^{-/-}$ mice were purchased from the Jackson Laboratory (Bar Harbor, ME). At 8 wk of age, mice were started on a Western diet (WD) containing 40% calories from fat, 43% calories from carbohydrate, and 17% calories from protein (D12079B; Research Diets, New Brunswick, NJ). Mice were exposed to e-cigarette aerosol from bluCig PLUS Classic tobacco e-cigarettes containing 2.4% nicotine (purchased on the bluCig website) for 12 wk. Control mice were exposed to a bluCig PLUS e-cigarette containing Gold Leaf tobacco (0% nicotine) or saline aerosol (74) (Afasci, Burlingame, CA). Classic tobacco and Gold Leaf tobacco flavors are similar except for their nicotine content.

E-cigarette aerosol generation and rodent exposure system. We developed an e-cigarette aerosol generation and free-moving rodent exposure system (patent number PCT/US17/54133). The system includes an aerosol exposure chamber that holds up to five free-moving mice, e-cigarette holders, and an e-cigarette activation control unit. The device is connected to a pressurized air source, and we adjust the air pressure that activates the e-cigarettes and generates an appropriate flow of e-cigarette aerosol to the mouse exposure cage. E-cigarette aerosol concentration in air is controlled by the number of activated e-cigarettes and the air pressure. The air pressure and flow are monitored with pressure gauges and flow meters during experiments. Since e-cigarette activation is intermittent, fresh air flow is maintained when e-cigarette aerosol flow stops, which eliminates residue aerosol from the chamber and provides fresh air for normal mice breathing. Our chronic intermittent e-cigarette exposure protocol was: an activation for 4 s is a puff; 8 puffs per vaping episode with an interpuff interval of 25 s; 1 vaping episode every 30 min. Mice were exposed to intermittent e-cigarette aerosol (24 vaping episodes) for 12 h ("on") from 2100 to 0900 the next morning. During the 12-h "off" period from 0900 to 2100, mice were returned to their home cages without any aerosol exposure. Food and water were provided ad libitum during both light and dark phases.

Saline aerosol, as a control for e-cigarette aerosol, was generated with an aerosol generation and rodent exposure system described before (73, 74). This system is now commercially available (Afasci, Burlingame, CA). The aerosol particle size distribution was shown to be within the respirable size range recommended by the United States Environmental Protection Agency (79) and the Organization for Economic Co-operation and Development (62).

Serum FFA quantification. For tail blood collection, mice were fasted for 16 h. For serum preparation, the blood was allowed to clot before centrifugation at 10,000 *g* for 10 min. FFA levels were quantified using the manufacturer's protocol (BioVision, cat. no. K612-100).

Echocardiography. Following the 12-wk exposure period, mice were screened by echocardiography at the Mouse Physiology Core Laboratory at the UCLA Department of Physiology. Cardiac function was evaluated by noninvasive ultrasound echocardiography under light isoflurane sedation (0.5–1.0%) to prevent movement and cardiodepression. Data were acquired using a two-dimensional-guided M-Mode and spectral Doppler imaging with a Siemens Acuson Sequoia Model C256 equipped with a 15L8 15-MHz probe (Siemens Medical Solutions, Malvern, CA). Mice were evaluated to obtain heart dimension and function measurements, including left ventricle (LV) chamber size, wall thickness, end-diastolic dimension, end-systolic dimension, LV fractional shortening, velocity of circumferential fiber shortening, and LV ejection fraction (70, 72).

Measurements of cotinine levels. Following the 12-wk experiment, and 15–60 min after the last exposure to the e-cigarette aerosol, mouse blood was collected, and plasma was used for determination of cotinine levels at the UCSF Clinical Pharmacology Laboratory using LC-LC/MS (39).

RNA-seq analysis. RNA was isolated from LVs ($n = 5$ in each group). RNA quality was assessed with an Agilent 2100 Bioanalyzer. RNA samples exhibited clear 28S and 18S rRNA peaks and demonstrated an RNA integrity number >8. Libraries for RNA-seq were prepared with KAPA Stranded RNA-Seq Kit. The workflow consists of mRNA enrichment, cDNA generation, and end repair to generate blunt ends, A-tailing, adaptor ligation, and PCR amplification. Different adaptors were used for multiplexing samples in one lane. Sequencing was performed on Illumina HiSeq 3000 for a single-read 50 run. Data quality check was done on Illumina SAV. Demultiplexing was performed using the Illumina Bcl2fastq2 v 2.17 program.

Reads were first mapped to the latest UCSC transcript set using Bowtie2 version 2.1.0 (43), and the gene expression level was estimated using RSEM v1.2.15 (48). Trimmed mean of M-values was used to normalize the gene expression. Differentially expressed genes were identified using the edgeR program (69). Genes showing altered expression with $P < 0.05$ and > 1.5-fold changes were considered differentially expressed. Differentially expressed genes were analyzed to predict changes in canonical pathways using Ingenuity Pathway Analysis (IPA) software (Ingenuity Systems). The RNA-seq data have been deposited in the NCBI Sequence Read Archive under BioProject accession number PRJNA504919 (https://www.ncbi.nlm.nih.gov/sra/PRJNA504919).

Real-time PCR. Left ventricular RNA from mice treated with saline aerosol, e-cigarette (0%), or e-cigarette (2.4%) was extracted with TRIzol Reagent (Invitrogen) using a Pyrex homogenizer. A 260/280 ratio greater than 1.9 using NanoDrop 2000 (Thermo Fisher Scien-

tific) was considered as purified RNA. The cDNA was prepared using the High Quality RNA-to-cDNA Kit (Applied Biosystems). The quantitative PCR (qPCR) was done using Step-One plus RT-PCR system (Life Technology) with an SYBR Green PCR Master Mix (Applied Biosystems). All reactions were analyzed in triplicate, and 4–5 mice from each group were tested. Data were normalized to 18S RNA transcripts using the $2^{-\Delta\Delta Ct}$ method for relative quantitation of gene expression. The primers used for real-time PCR are as follows: COL1a1: forward (F) 5′-GCGAAGGCAACAGTCGATTC-3′ and reverse (R) 5′-CCCAAGTTCCGGTGTGACTC-3′; COL3a1: (F) 5′-GGGTTTCCCTGGTCCTAAAG-3′ and (R) 5′-CCTGGTTTC-CCATTTTCTCC-3′; collagen type V α3 (COL5a3): (F) 5′-GAT-GAACCAGAAACCCCTGC-3′ and (R) 5′-AGCACCAGGAAA-GATCTGGA-3′; DNA damage inducible transcript 4 like (Ddit4L): (F) 5′-CTTCAGCGTCTGGTGAAATCC-3′ and (R) 5′-ATGCTG-GCCGTGTTCTTACTG-3′; harakiri: (F) 5′-GAAACCCTGTGTC-CTTGGAG-3′ and (R) 5′-TGTCTGTGTTTCCACCATCA; neuronal PAS domain protein 2 (Npas2): (F) 5′-TCCCTGGTAACACTCG-GAAA-3′ and (R) 5′-GCCATCTAATGCCTCCAACA-3′; period circadian protein homolog 2 (Per2): (F) 5′-TGTTCCGACATGCTT-GCG-3′ and (R) 5′-GAAACAGCTTCCTCTGCTCCAG-3′; period circadian protein homolog 3 (Per3): (F) 5′-GTGTACACAGTGTG-CAAGCAAACA-3′ and (R) 5′-ACGGCCGCGAAGGTATCT-3′; stearoyl-CoA desaturase 1 (SCD1): (F) 5′-CCTTCCCCTTCGAC-TACTCTG-3′ and (R) 5′-GCCATGCAGTCGATGAAGAA-3′; tissue inhibitor of metalloproteinase 4 (Timp4): (F) 5′-ACTTGCTAT-GCAGTGCCATG-3′ and (R) 5′-TCGGTACCAGCTGCAGATG-3′; TNF RSM 12A: (F) 5′-CTGGTTTCTAGTTTCCTGGT-3′ and (R) 5′-CTTGTGGTTGAAAGAGTCTG-3′; WNT1-inducible signaling pathway protein 2 (Wisp2): (F) 5′-GTACCTGGATGGGGAG-ACCT-3′ and (R) 5′-GTTGGATACTCGGGTGGCTA-3′; and 18s: (F) 5′-GTAACCCGTTGAACCCCATT-3′ and (R) 5′-CCATC-CAATCGGTAGTAGCG.

MtDNA damage assay. Briefly, in this assay, the polymerase binds to undamaged DNA (mice receiving saline aerosol) and replicates a full-length PCR product. In the presence of damaged DNA [mice receiving e-cigarettes (2.4%)], the polymerase has a higher probability to stop, preventing full replication, and thereby resulting in decreased amplification. The "long PCR" amplification product (16,000 bp) has increasing probability for detection of mtDNA lesions. This fragment was normalized to mtDNA copy number via a "short-range" PCR amplification product (80 bp) of the mitochondrial genome in which the polymerase has a low probability of having lesions (because of its small amplification size). Genomic DNA was isolated from ventricular of ApoE$^{-/-}$ mice using the Genomic-tip 20/G and Qiagen DNA Buffer Set (Qiagen, MD) as per the manufacturer's instruction. Eluted DNA was incubated with isopropanol overnight at 80°C and centrifuged 12,000 *g* for 60 min. DNA was washed with 70% ethanol and dissolved in Tris-EDTA buffer. For long PCR product, we used the following primer sequences: 5′-CCCAGCTACTACCATCATTCA-AGTAG-3′ for long forward and 5′-GAGAGATTTTATGGGTGTA-ATGCGGTG-3′ for long backward. The short PCR product was amplified using the following primer sequences: 5′-GCAAATC-CATATTCATCCTTCTCAAC-3′ for short forward and the reverse primer sequence was the same as long backward (57, 67). For each primer set, the reaction was conducted in triplicate in a 25-ml final volume containing 1X SYBR green master mix, 500 nM each primer, and 4 ng of genomic DNA. Lesion frequency per amplicon was determined assuming a random distribution of lesions calculated as: lesion rate $= 1 - 2^{(\Delta CT\ long\ -\ \Delta CT\ short)} \times$ (10,000 bp/16,000 bp) (64).

Electron microscopy. For transmission electron microscopic studies, portions of the LVs were fixed in 2.5% glutaraldehyde in 0.05 M sodium cacodylate buffer (pH 7.4) and then further diced into small pieces, postfixed in 1% osmium tetroxide, and embedded in Epon 812 as described previously (23, 76). Thin sections from selected tissue blocks were cut with an LKB Ultramicrotome, stained with uranyl acetate and lead citrate, and examined with a Hitachi electron microscope (Hitachi, Indianapolis, IN). Special emphasis was given to key structural changes associated with dilated cardiomyopathy (66).

Atherosclerotic lesions. To analyze atherosclerotic lesions, the basal portion of the heart and proximal aorta were embedded in OCT compound (Tissue-Tek, Elkhart, IN), frozen on dry ice, and then stored at −80°C until sectioning. Serial 10-μm-thick cryosections (50–60 sections per mouse) were cut through the ventricle from the appearance to the disappearance of the aortic valves. Every other section was collected on poly-D-lysine-coated slides. The sections were stained with Oil Red O and counterstained with hematoxylin and fast green for visualization of atherosclerotic lesions. Lesion areas were quantified with Image-Pro Plus (5). Briefly, the lesions were circled, and the area of each lesion for the quantified section on the slide was exported to a spreadsheet (in μm^2). This was repeated for each of the slides, and the sum of the lesions area was calculated (μm^2/section) for each mouse.

Lipid peroxidation. Thiobarbituric acid reactive substances assay to measure malondialdehyde (MDA) in tissue was determined by the procedure described by the manufacturer (700870, Cayman Chemical, Ann Arbor, MI).

Statistical analyses. Statistical analyses were performed using Prism 8 (GraphPad Software, San Diego, CA). Data are expressed as means ± SE. The effects of e-cigarettes (2.4%) versus saline or e-cigarette (0%) were determined using two-way, repeated-measures ANOVA, followed by the Holm-Sidak method for multiple comparison (1).

RESULTS

Characterization of ApoE$^{-/-}$ mice exposed to saline aerosol, e-cigarette (0%), and e-cigarette (2.4%). ApoE$^{-/-}$ mice on a WD were exposed to saline aerosol and e-cigarette with nicotine (2.4%) and without nicotine (0%) for 12 wk. The solvents in e-cigarettes, including propylene glycol and glycerol, have been shown to produce free radicals in a temperature-dependent manner (13). Therefore, non-nicotine e-cigarette (0%) was used to control for the effects of the solvents of nicotine e-cigarette (2.4%) on the heart. After 12 wk of treatment with e-cigarette (2.4%), the concentration of plasma cotinine was 611 ± 54 ng/ml. This is in the range of heavy smokers who had smoked at least 18 cigarettes a day (11). In contrast, the concentration of plasma cotinine in mice that received saline aerosol and e-cigarette (0%) was undetectable.

Figure 1*A* shows that mice exposed to e-cigarette (2.4%) had increased levels of serum FFAs in comparison with both saline-treated ($P < 0.01$) and e-cigarette (0%)-treated mice ($P < 0.05$). In contrast, FFA levels of mice exposed to saline aerosol and e-cigarette (0%) were similar. Although, in the first 8 wk, there was a trend toward a decrease in body weight in mice treated with e-cigarette (2.4%), overall there was not a statistically significant difference in body weight among these groups (Fig. 1*B*).

Echocardiographic analysis from mice treated with e-cigarettes. We assessed the cardiac function in mice treated with saline aerosol, e-cigarette (0%), and e-cigarette (2.4%) in ApoE$^{-/-}$ mice using echocardiographic analysis. M-mode measurements of LV dimensions revealed no differences among saline aerosol, e-cigarette (0%), and e-cigarette (2.4%) -exposed groups (Table 1). Similarly, heart/body ratio and heart rate were unchanged after 12 wk of e-cigarette treatment (Table 1). LV fractional shortening, LV ejection fraction, and velocity of circumferential fiber shortening were all decreased in mice exposed to e-cigarette (2.4%) compared with those in saline

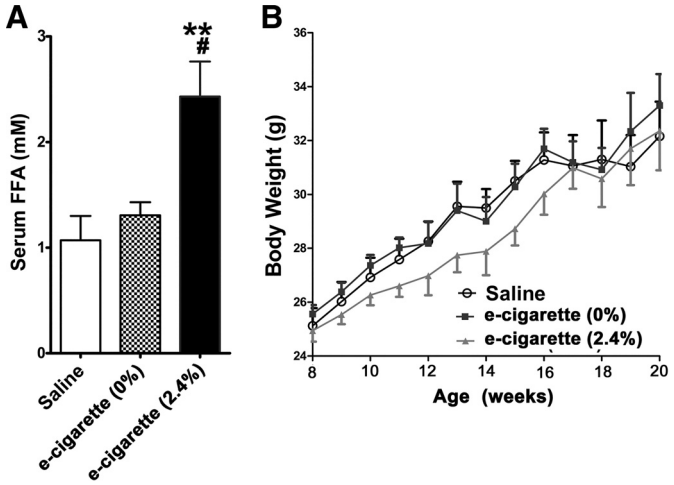

Fig. 1. Effects of electronic cigarettes (e-cigarettes) on serum free fatty acid (FFA) levels (*A*) and body weight (*B*) in apolipoprotein-E knockout mice. All values are means ± SE; $n = 5$ per group; saline vs. e-cigarette (2.4%), $^{**}P < 0.01$; e-cigarette (0%) vs. e-cigarette (2.4%), $\#P < 0.05$. Time by group interaction was not significant for the effects of e-cigarettes on body weight.

aerosol- and e-cigarette (0%)-treated groups. We observed no difference between e-cigarette (2.4%) versus saline aerosol and e-cigarette (0%) in the left ventricular diastolic function parameters such as peak early diastolic (*E*), atrial filling velocity (*A*), and *E*/*A* ratio. Therefore, at 12 wk, mice exposed to e-cigarette (2.4%) developed impaired ventricular systolic function without change in diastolic function. The lack of an effect of e-cigarette (0%) shows that nicotine is necessary for the induction of systolic dysfunction induced by e-cigarette (2.4%). In the $ApoE^{-/-}$ mice before the treatment, we did not observe any significant difference in the echocardiographic data among various treatment groups.

RNA-seq analysis from ventricles of mice treated with e-cigarettes with (2.4%) and without nicotine (0%). To understand this phenotype with greater details, e-cigarette (2.4%) and saline aerosol mice were transcriptome profiled by RNA-seq. Of the 24,054 genes analyzed, 109 were differentially expressed. Figure 2*A* shows the 2-dimensional hierarchical clustering of 109 differentially expressed genes with $P < 0.05$ and >1.5-fold changes (for full list of genes, see Tables 2 and 3). In Fig. 2*A*, each column represents one mouse and each row a gene probe set. Probe set signal values were normalized to the mean across the animals, and the relative level of gene expression is depicted from the most downregulated (green) to the most upregulated (red), according to the scale shown on the left. Of the 109 genes differentially expressed in e-cigarette (2.4%) hearts, 48 (44%) were upregulated [for full list, see Table 2, saline aerosol vs. e-cig (2.4%) column] and 61 (56%) were downregulated [for full list, see Table 3, saline vs. e-cig (2.4%) column]. The RNA-seq examination using IPA software revealed dysregulation of inflammatory, circadian rhythm, and leukocyte extravasation signaling in e-cigarette-exposed hearts (Table 4). The proinflammatory phenotype induced by e-cigarette (2.4%) was associated with an increase in expression of inflammatory molecules Col5a3 (59), tumor necrosis factor receptor superfamily member 12a (TNFRSF12A) (61), and selectin E (31). In terms of circadian rhythm genes, RNA-seq data showed decreased expression in Per2 and Per3 genes and increased expression of NPAS2 and glutamate ionotropic receptor NMDA type subunit 2C genes. Furthermore, RNA-seq profiling showed that myocardial damage induced by e-cigarette (2.4%) was associated with changes in leukocyte extravasation signaling. Taken together, the gene expression fingerprint shows a cardiac proinflammatory phenotype induced by nicotine e-cigarette (2.4%) in the $ApoE^{-/-}$ model. We also tested by qPCR two genes that did not have a change in the RNA-seq analysis, collagen type I and collagen type III (Fig. 3). We did not observe a change in collagen type I/collagen type III ratio, a marker for cardiac fibrosis, with this qPCR data (data not shown). Therefore, qPCR analysis of collagen suggests the induction of inflammatory changes without fibrosis by e-cigarette (2.4%).

To understand which genes were nicotine independent, we studied the transcriptomic changes induced by saline aerosol versus e-cigarettes (0%). We observed 226 cardiac genes that were differentially expressed between saline and e-cigarette (0%). Figure 2*B* shows the two-dimensional hierarchical clustering of the comparison between saline versus e-cigarettes (0%). The Venn diagram (Fig. 2*D*) depicts 29 differentially expressed genes that were similarly expressed ($P < 0.05$, >1.5-fold changes, and in similar direction) in the saline-treated group when compared with non-nicotine e-cigarette (0%)- or nicotine e-cigarette (2.4%)-exposed groups. The fold changes of these 29 nicotine-independent genes have been underlined in Tables 2 and 3 [saline vs. e-cigarette (0%) column].

To understand which genes were nicotine dependent, we studied the transcriptomic changes induced in the heart by treatment with e-cigarette (0%) versus e-cigarette (2.4%). We found 241 genes that were differentially expressed between e-cigarette (0%)- and cigarette (2.4%)-exposed hearts. Figure 2*C* shows the two-dimensional hierarchical clustering of the comparison between e-cigarettes (0%) versus e-cigarettes

Table 1. *Echocardiographic data of mice treated with e-cigarette (2.4% nicotine), e-cigarette (0% nicotine), and saline at 12 wk*

	Saline	E-cigarette (0%)	E-cigarette (2.4%)
VST, mm	0.50 ± 0.3	0.49 ± 0.4	0.53 ± 0.4
EDD, mm	4.16 ± 0.24	4.42 ± 0.50	4.06 ± 0.21
PWT, mm	0.53 ± 0.03	0.49 ± 0.02	0.53 + 0.03
ESD, mm	2.72 ± 0.26	2.92 ± 0.42	2.96 ± 0.15
Ao-ET, ms	50 ± 5	48 ± 2	55 + 2
HR	535 ± 45	479 ± 99	479 ± 36
LV% FS	35 ± 3	34 ± 4	27 ± 1**,##
VCF	7.1 ± 1.2	7.05 ± 0.9	5.0 ± 0.2**,##
LVEF	69 ± 4	70 ± 7	60 ± 2*,#
LV mass	72 ± 8	76 ± 16	71 ± 8
E	0.71 ± 0.1	0.82 ± 0.2	0.68 ± 0.1
A	0.36 ± 0.1	0.49 ± 0.1	0.34 ± 0.1
E/*A* ratio	2.0 ± 0.1	1.65 ± 0.2	2.1 ± 0.1
H/B ratio	2.27 ± 0.45	2.40 ± 0.42	2.26 ± 0.32

Values are means ± SD; statistical analysis by covariant analysis. $n = 5$ per group, saline vs. e-cigarette (2.4%). *A*, atrial systole; Ao-ET, aortic ejection time; *E*, early diastole (LV filling); e-cigarette, electronic cigarette; EDD, end-diastolic dimension; ESD, end-systolic dimension; H/B ratio, heart wt/body wt ratio; HR, heart rate; LVEF, left ventricle ejection fraction; LV% FS, left ventricle fractional shortening; LV mass, left ventricle mass; PWT, posterior wall thickness; VCF, velocity of circumferential fiber shortening; VST, ventricular septal thickness. $^{*}P < 0.05$, $^{**}P < 0.01$, e-cigarette (0%) vs. e-cigarette (2.4%), $\#P < 0.05$, $\#\#P < 0.01$.

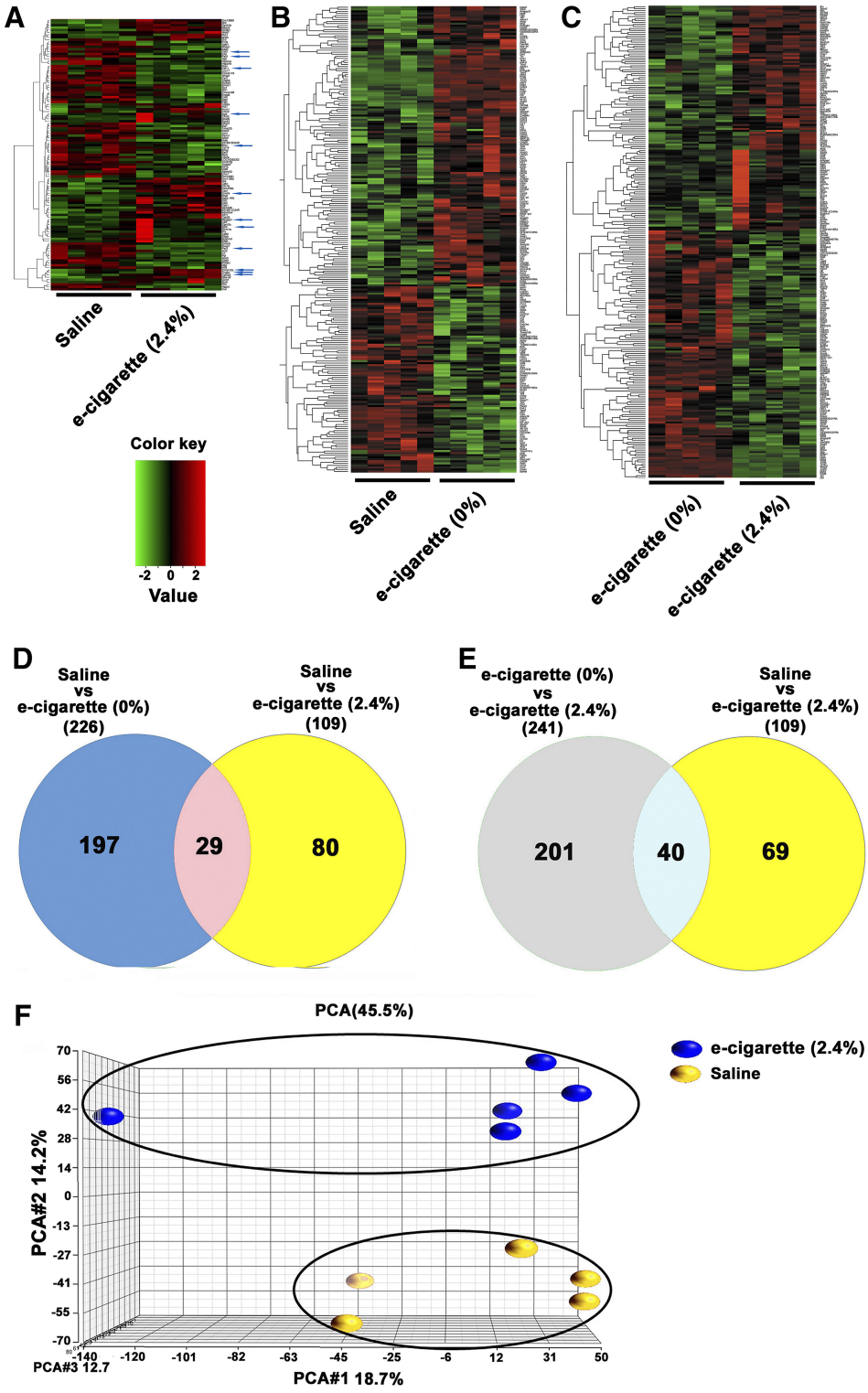

Fig. 2. Transcriptomic changes induced by electronic cigarette (e-cigarette) (0%) and e-cigarette (2.4%). *A*: 2-dimensional hierarchical clustering showing 109 differentially expressed genes between saline and e-cigarette (2.4%). Blue arrows point to genes associated with the Ingenuity Pathway Analysis. *B*: 2-dimensional hierarchical clustering showing 226 differentially expressed genes between saline and e-cigarette (0%). *C*: 2-dimensional hierarchical clustering showing 241 differentially expressed genes between e-cigarette (0%) and e-cigarette (2.4%). *A–C*: each column represents an animal and each row a gene probe set. Probe set signal values were normalized to the mean across. The relative level of gene expression is depicted from the most downregulated (green) to the most upregulated (red), according to the scale shown on the *left*. *D*: Venn diagram representing data summary of differentially expressed genes in saline vs. e-cigarette (0%) and saline vs. e-cigarette (2.4%). *E*: Venn diagram representing data summary of differentially expressed genes in e-cigarette (0%) vs. e-cigarette (2.4%) and saline vs. e-cigarette (2.4%). *F*: principal component analysis (PCA) of heart samples treated with saline (yellow) and heart samples treated with e-cigarette (2.4%), which are independently clustered.

(2.4%). As shown in the Venn diagram (Fig. 2*E*), there were 40 genes showing the similar changes ($P < 0.05$, >1.5-fold changes, and in the similar direction) caused by nicotine e-cigarette (2.4%) compared with non-nicotine e-cigarette (0%) or saline aerosol. The fold changes of these 40 nicotine-dependent genes are now marked in boldface in Tables 2 and 3 [e-cigarette (0%) vs. e-cigarette (2.4%) column].

To determine whether saline aerosol and e-cigarette (2.4%) RNA-seq expression data have a clear segregation, we performed principal component analysis (PCA). Figure 2*F* shows PCA performed on filtered gene expression data, with circles representing individual samples that are visualized according to treatment. Figure 2*F* shows that each treatment [saline aerosol or e-cigarette (2.4%)] is distinctly clustered. Therefore,

Table 2. *Upregulated genes in RNA-seq data*

		Saline vs. E-cigarette (2.4%)		Saline vs. E-cigarette (0%)		E-cigarette (0%) vs. E-cigarette (2.4%)	
Gene Symbol	Name	Fold change	*P* value	Fold change	*P* Value	Fold change	*P* value
Npas2	Neuronal PAS domain protein 2	1.78	3.97×10^{-8}	−1.62	1.10×10^{-4}	**2.90**	$\mathbf{2.52 \times 10^{-18}}$
Dixdc1	DIX domain containing 1	1.54	9.50×10^{-7}	1.88	2.96×10^{-11}	−1.35	0.13
Gm13889	Predicted gene 13889	1.63	7.83×10^{-6}	1.10	0.45	1.49	0.00
Mt2	Metallothionein 2	1.82	3.21×10^{-5}	1.33	0.03	−1.12	0.01
Hba-a2	Hemoglobin α, adult chain 2	1.77	4.36×10^{-5}	1.85	3.29×10^{-4}	−1.04	0.82
Col5a3	Collagen, type V, α3	1.56	4.70×10^{-5}	−1.05	0.69	**1.64**	$\mathbf{1.58 \times 10^{-5}}$
Igfals	Insulin-like growth factor binding protein, acid labile subunit	1.68	1.18×10^{-4}	1.34	0.05	1.26	0.10
Ccnf	Cyclin F	2.36	2.82×10^{-4}	1.33	0.24	**1.78**	$\mathbf{7.97 \times 10^{-3}}$
Timp4	Tissue inhibitor of metalloproteinase 4	1.55	4.46×10^{-4}	1.07	0.61	1.45	0.004
Dynlt1b	Dynein light chain Tctex-type 1B	1.51	6.64×10^{-4}	1.40	0.01	1.08	0.55
Nrn1	Neuritin 1	2.06	1.04×10^{-3}	1.53	0.08	1.35	0.21
Socs3	Suppressor of cytokine signaling 3	3.03	1.25×10^{-3}	1.52	0.18	**1.99**	$\mathbf{2.94 \times 10^{-2}}$
Tnfrsf12a	Tumor necrosis factor receptor superfamily, member 12a	1.55	1.26×10^{-3}	−1.02	0.90	**1.59**	$\mathbf{1.05 \times 10^{-3}}$
Adamts4	A disintegrin-like and metallopeptidase with thrombospondin type 1 motif, 4	2.06	1.69×10^{-3}	−1.24	0.37	**2.56**	$\mathbf{5.68 \times 10^{-5}}$
Gprc5a	G protein-coupled receptor, family C, group 5, member A	3.30	3.30×10^{-3}	−1.47	0.32	**4.86**	$\mathbf{5.47 \times 10^{-5}}$
Rasgrp1	RAS guanyl-releasing protein 1	2.61	3.56×10^{-3}	1.30	0.40	**2.02**	$\mathbf{1.77 \times 10^{-2}}$
Sema5b	Semaphorin 5B	1.55	5.58×10^{-3}	1.13	0.38	1.37	0.02
Cdo1	Cysteine dioxygenase 1, cytosolic	2.43	5.60×10^{-3}	1.77	0.06	1.38	0.27
Grin2c	Glutamate receptor, ionotropic, NMDA2C (ε3)	1.88	5.60×10^{-3}	1.07	0.77	**1.76**	$\mathbf{1.24 \times 10^{-2}}$
Cd4	CD4 antigen	2.92	5.86×10^{-3}	1.15	0.71	**2.56**	$\mathbf{8.02 \times 10^{-3}}$
Chst3	Carboh+++ydrate (chondroitin 6/ keratan) sulfotransferase 3	1.79	6.07×10^{-3}	1.21	0.32	1.48	0.04
Mki67	Antigen identified by monoclonal antibody K_i 67	1.51	8.11×10^{-3}	1.97	3.83×10^{-5}	−1.30	0.10
Kcnc1	Potassium voltage gated channel, Shaw-related subfamily, member 1	1.55	8.33×10^{-3}	−1.18	0.38	**1.83**	$\mathbf{8.67 \times 10^{-4}}$
Top2a	Topoisomerase (DNA) IIα	1.65	9.06×10^{-3}	1.58	0.02	1.04	0.82
Akap5	A kinase (PRKA) anchor protein 5	1.57	9.40×10^{-3}	1.84	1.72×10^{-4}	−1.16	0.34
Hrk	Harakiri, BCL2 interacting protein (contains only BH3 domain)	1.74	1.10×10^{-2}	1.00	0.99	**1.74**	$\mathbf{6.80 \times 10^{-3}}$
2210011C24Rik	RIKEN cDNA 2210011C24 gene	1.55	1.13×10^{-2}	1.02	0.91	**1.52**	$\mathbf{5.94 \times 10^{-3}}$
Gm11992	Predicted gene 11992	1.69	1.19×10^{-2}	−1.00	0.98	**1.70**	$\mathbf{1.05 \times 10^{-2}}$
Kif11	Kinesin family member 11	1.61	1.32×10^{-2}	1.79	2.73×10^{-3}	−1.11	0.59
Prc1	Protein regulator of cytokinesis 1	1.61	1.34×10^{-2}	1.80	1.12×10^{-3}	−1.02	0.75
Gvin1	GTPase, very large interferon inducible 1	1.60	1.44×10^{-2}	1.17	0.42	1.37	0.11
Nnat	Neuronatin	1.95	1.46×10^{-2}	1.75	2.81×10^{-2}	1.12	0.65
Scd1	Stearoyl-Coenzyme A desaturase 1	2.12	1.52×10^{-2}	1.19	0.52	**1.78**	$\mathbf{3.65 \times 10^{-2}}$
Ccl2	Chemokine (C-C motif) ligand 2	1.81	1.86×10^{-2}	1.82	1.55×10^{-2}	−1.00	0.99
Sele	Selectin, endothelial cell	2.28	2.01×10^{-2}	1.58	0.16	1.45	0.24
Epb4.1l4b	NA	1.53	2.71×10^{-2}	1.32	0.12	1.16	0.39
Prx	Periaxin	2.13	2.77×10^{-2}	−1.19	0.59	**2.53**	$\mathbf{3.21 \times 10^{-3}}$
Fam150b	Family with sequence similarity 150, member B	1.67	2.80×10^{-2}	−1.34	0.22	2.23	0.00
Olfr78	Olfactory receptor 78	1.60	3.01×10^{-2}	1.17	0.48	1.38	0.11
Cdc20	Cell division cycle 20	1.63	3.15×10^{-2}	1.60	3.20×10^{-2}	1.02	0.92
Scgb1a1	Secretoglobin, family 1A, member 1 (uteroglobin)	3.31	3.21×10^{-2}	−11.79	0.00229	**39.22**	$\mathbf{2.67 \times 10^{-5}}$
Itgal	Integrin αL	1.66	4.08×10^{-2}	−1.16	0.54	**1.92**	$\mathbf{6.21 \times 10^{-3}}$
Cd22	CD22 antigen	2.31	4.35×10^{-2}	−1.14	0.74	**2.63**	$\mathbf{1.35 \times 10^{-2}}$
Cntn2	Contactin 2	2.00	4.45×10^{-2}	1.01	0.98	1.99	0.11
Scnn1a	Sodium channel, nonvoltage-gated 1α	2.04	4.50×10^{-2}	1.06	0.86	**1.94**	$\mathbf{3.91 \times 10^{-2}}$

Continued

PCA indicates a differential transcriptional response to saline aerosol and e-cigarette (2.4%) in the heart of $ApoE^{-/-}$ mice.

Validation by qPCR. To validate the results of the genome-wide analysis, we performed qPCR on a set of genes altered by e-cigarette (2.4%) as shown in RNA-seq. We analyzed the RNA expression of hearts exposed to saline, e-cigarette (0%), and e-cigarette (2.4%). Figure 3 shows 8 genes from 10 with a significant change in the RNA-seq data [e-cigarette (2.4%) vs. saline or e-cigarette (0%)] that showed a significant change ($P < 0.05$) in the qPCR data for e-cigarette (2.4%). Since we studied the phenotype dependent of nicotine, we validated by qPCR eight genes that were differentially expressed in saline

Table 2.—*Continued*

Gene Symbol	Name	Saline vs. E-cigarette (2.4%) Fold change	Saline vs. E-cigarette (2.4%) *P* value	Saline vs. E-cigarette (0%) Fold change	Saline vs. E-cigarette (0%) *P* Value	E-cigarette (0%) vs. E-cigarette (2.4%) Fold change	E-cigarette (0%) vs. E-cigarette (2.4%) *P* value
Cdk1	Cyclin-dependent kinase 1	1.63	4.54×10^{-2}	1.57	4.93×10^{-2}	1.04	0.85
Irx2	Iroquois-related homeobox 2 (Drosophila)	1.56	4.83×10^{-2}	−1.15	0.65	1.79	0.05
cl7	Chemokine (C-C motif) ligand 7	1.77	4.96×10^{-2}	2.48	5.30×10^{-4}	−1.39	0.18

Saline vs. electronic cigarette (e-cigarette) (2.4%) columns show the fold changes and *P* value of the differentially upregulated genes between saline aerosol and e-cigarette (2.4%). Saline vs. e-cig (0%) columns show all the changes between saline and e-cigarette (0%) for the listed genes. In the saline vs. e-cig (0%) columns, the changes underlined are similar to column saline vs. e-cigarette (2.4%). The similar upregulation gene expression (underlined) suggests that the changes saline vs. e-cigarette (2.4%) column are nicotine independent for the associated gene. E-cigarette (0%) vs. e-cigarette (2.4%) columns show all the changes and between e-cigarette (0%) and e-cigarette (2.4%) in the listed genes. In the e-cigarette (0%) vs. e-cigarette (2.4%) columns, the changes marked in boldface are similar to the saline vs. e-cigarette (2.4%) column. These similar changes in gene expression (in boldface) suggest that changes in the saline vs. e-cigarette (2.4%) column are dependent of nicotine for the associated genes. Genes showing altered expression with $P < 0.05$, >1.5-fold changes in the same direction, were considered differentially expressed in similar way.

aerosol versus e-cigarette (2.4%) and e-cigarette (0%) versus e-cigarette (2.4%) but not in saline aerosol versus e-cigarette (0%) (Tables 2 and 3, in boldface). For example, SCD1, the rate-limiting enzyme in synthesis of monounsaturated fatty acids was increased in hearts of mice exposed to e-cigarette (2.4%) in comparison with saline ($P < 0.01$) and e-cigarette (0%) ($P < 0.05$). Col5a3, a gene activated in the inflammatory process (59), was increased in e-cigarette (2.4%)-treated mice in comparison with saline ($P < 0.05$) and e-cigarette (0%) ($P < 0.05$). TNFRSF12A/Fn14, a gene associated with ROS induction in vascular damage (52) and apoptosis (68), was increased in e-cigarette (2.4%)-treated mice in comparison with saline ($P < 0.05$) and e-cigarette (0%) ($P < 0.05$). Hrk mRNA, a proapoptotic gene activated by cigarettes (7, 22, 38), was increased in hearts of mice exposed to e-cigarette (2.4%) in comparison with saline ($P < 0.01$) and e-cigarette (0%) ($P < 0.01$). Consistent with the fact that the onset of systolic dysfunction is associated with changes in circadian genes in the heart (21), Npas2, a gene that controls glucose and lipid metabolism (29), was increased in comparison with saline ($P < 0.05$) and e-cigarette (0%), whereas Per2 and Per3 were decreased in e-cigarette (2.4%)-treated mice in comparison with saline ($P < 0.05$) and e-cigarette (0%) ($P < 0.05$ for Per2 and $P < 0.01$ for Per3). Wisp2/CCN5, a cardiac protective gene, was downregulated in mice exposed to e-cigarette (2.4%) in comparison with saline ($P < 0.05$) and e-cigarette (0%) ($P < 0.05$).

For additional validation, we performed qPCR analysis of genes that were differentially expressed in saline aerosol-treated versus e-cigarette (2.4%)-treated but not in saline aerosol versus e-cigarette (0%) or e-cigarette (0%) versus e-cigarette (2.4%)-treated (Tables 2 and 3, regular type). As expected, cardiac expression of TIMP4, a gene that controls extracellular matrix remodeling in the heart (40), and DDIT4L/REDD2, an inhibitor of mammalian target of rapamycin signaling (58), were not different between e-cigarette (2.4%) versus e-cigarette (0%) or saline-exposed mice. Taken together, RNA-seq analysis and its validation by qPCR unveils that e-cigarette (2.4%) induced inflammatory and circadian rhythm signaling dysregulation in ApoE$^{-/-}$ mice.

E-cigarette (2.4%) induces cardiac ultrastructural abnormalities. Next, we tested if e-cigarette (2.4%) induced systolic dysfunction coupled with altered gene expression was associated with structural changes. CMs from saline-treated ApoE$^{-/-}$ mice showed normal myofibrillar architecture and sarcomeric pattern with normal nuclei and abundant mitochondria as shown by electron microscopy (Fig. 4*A*). In contrast, CMs from e-cigarette (2.4%)-exposed mice exhibited varying degrees of both nuclear as well as cytoplasmic abnormalities (Fig. 4, *B–F*), indicative of cardiomyopathy (66). The most predominant nuclear abnormalities included shrunken nuclei with chromatin condensation and fragmentation, as seen in apoptosis (Fig. 4, *B* and *C*), and nuclear malformation with extensively convoluted nuclear membrane (Fig. 4, *D* and *E*). The most prominent cytoplasmic abnormalities were myofibrillar derangement, thinning, and destruction (Fig. 4, *B–F*). Other cytoplasmic abnormalities included intramyocardial lipid accumulation and mitophagy (Fig. 4, *G–I*).

Effect of e-cigarettes (2.4%) on ROS generation and mtDNA mutations. Inflammation and ROS are important in induction of atherosclerotic lesions and cardiomyopathy (12, 81). Increase in mitochondrial ROS can lead to mtDNA damage (45). Figure 5*A* shows that e-cigarette (2.4%) induced an increase in MDA levels in comparison with saline ($P < 0.05$) or e-cigarette (0%) ($P < 0.05$). There was an increase in 0.96 lesion/10,000 bases ($P < 0.05$) in mice exposed to e-cigarette (2.4%) compared with that of saline-exposed mice (lesions set at 0) or e-cigarette (0%) ($P < 0.01$). Therefore, e-cigarette (2.4%) treatment leads to ROS generation and mtDNA damage.

E-cigarettes induce atherosclerotic lesion formation. To determine the effects of e-cigarettes (2.4%) on atherosclerotic lesion formation, we performed Oil Red O staining counterstained with hematoxylin and fast green. E-cigarette (2.4%) administration resulted in an increase in atherosclerotic lesions in the aortic root (Fig. 6*A*). Quantification of the lesion area with Image-Pro Plus of e-cigarette-treated versus saline aerosol-treated mice shows a significant increase in atherosclerotic formation ($53.6 \pm 7.5 \times 10^5$ μm^2 vs. $103.9 \pm 12.9 \times 10^5$ μm^2, $P < 0.01$; Fig. 6*B*).

DISCUSSION

In the current study, ApoE$^{-/-}$ mice were exposed to e-cigarette aerosol in a chronic intermittent protocol with 2.4% nicotine for 12 wk. At the end of the treatment period, plasma cotinine levels were in the range of plasma concentrations found in heavy smokers (10, 36), showing the relevance to human smokers and potentially e-cigarette users.

E-cigarettes produce an increase in IL-1β, IL-6, TNF-α, oxidative stress (37), ROS, and sympathetic predominance as

Table 3. *Downregulated genes in RNA-seq data*

Gene Symbol	Name	Saline vs. E-cigarette (2.4%)		Saline vs. E-cigarette (0%)		E-cigarette (0%) vs. E-cigarette (2.4%)	
		Fold change	*P* value	Fold change	*P* value	Fold change	*P* value
Tfrc	Transferrin receptor	−2.58	1.95×10^{-23}	−1.21	0.04	**−2.13**	**2.73×10^{-16}**
Svep1	Sushi, von Willebrand factor type A, EGF and pentraxin domain containing 1	−1.51	1.95×10^{-12}	1.05	0.61	**−1.58**	**2.01×10^{-6}**
Per3	Period circadian clock 3	−1.89	1.55×10^{-11}	1.09	0.38	**−2.04**	**1.11×10^{-13}**
Wisp2	WNT1 inducible signaling pathway protein 2	−2.22	1.22×10^{-10}	1.11	0.44	**−2.46**	**2.50×10^{-10}**
Smtnl2	Smoothelin-like 2	−1.53	6.54×10^{-10}	−1.20	0.01	−1.27	1.56×10^{-3}
Per2	Period circadian clock 2	−2.14	1.67×10^{-9}	1.12	0.44	**−2.39**	**2.19×10^{-8}**
Ano5	Anoctamin 5	−1.85	1.83×10^{-8}	−1.12	0.40	**−1.65**	**1.48×10^{-4}**
Cys1	Cystin 1	−2.00	2.75×10^{-7}	−1.73	2.07×10^{-4}	−1.15	0.34
Phlda1	Pleckstrin homology-like domain, family A, member 1	−1.65	3.56×10^{-7}	−1.52	1.21×10^{-2}	−1.08	0.64
Hsph1	Heat shock 105kDa/110kDa protein 1	−1.59	5.79×10^{-7}	1.16	0.244	**−1.84**	**2.10×10^{-6}**
Itgbl1	Integrin, β-like 1	−1.64	1.20×10^{-6}	1.02	0.872	**−1.66**	**2.20×10^{-5}**
Ppl	Periplakin	−1.52	2.62×10^{-6}	1.05	0.634	**−1.59**	**1.09×10^{-6}**
Wif1	Wnt inhibitory factor 1	−2.13	2.78×10^{-6}	1.01	0.854	−1.26	0.41
Hspa1b	Heat shock protein 1B	−4.04	4.19×10^{-6}	1.15	0.732	**−4.66**	**4.64×10^{-4}**
Ccr2	Chemokine (C-C motif) receptor 2	−1.71	2.51×10^{-5}	−1.77	2.36×10^{-6}	1.04	0.75
Hspa1a	Heat shock protein 1A	−3.60	2.58×10^{-5}	1.11	0.803	**−3.98**	**9.62×10^{-4}**
Fcrls	Fc receptor-like S, scavenger receptor	−1.57	2.66×10^{-5}	−1.24	0.041	−1.27	0.03
C7	Complement component 7	−1.65	3.21×10^{-5}	−1.16	0.261	−1.41	0.01
G0s2	G0/G1 switch gene 2	−1.56	3.39×10^{-5}	1.03	0.805	**−1.60**	**7.33×10^{-6}**
Srpx	Sushi-repeat-containing protein	−1.78	6.07×10^{-5}	−1.79	1.26×10^{-4}	1.01	0.94
Cilp	Cartilage intermediate layer protein, nucleotide pyrophosphohydrolase	−1.92	7.23×10^{-5}	1.08	0.661	**−2.07**	**5.54×10^{-5}**
Cngb3	Cyclic nucleotide gated channel β3	−1.76	1.27×10^{-4}	−1.43	0.012	−1.22	0.17
Smoc1	SPARC related modular calcium binding 1	−1.84	2.97×10^{-4}	−1.89	9.42×10^{-3}	1.03	0.91
Slc5a3	solute carrier family 5 (inositol transporters), member 3	−1.66	6.14×10^{-4}	−1.13	0.429	−1.47	0.01
H19	H19, imprinted maternally expressed transcript	−1.84	6.24×10^{-4}	−2.13	8.45×10^{-3}	1.16	0.60
Dbp	D site albumin promoter binding protein	−1.64	7.69×10^{-4}	3.20	1.81×10^{-16}	**−5.22**	**4.41×10^{-30}**
Lrrc17	Leucine rich repeat containing 17	−1.54	9.28×10^{-4}	−1.23	0.106	−1.25	0.08
Masp1	Mannan-binding lectin serine peptidase 1	−1.54	9.92×10^{-4}	−1.16	0.270	−1.32	0.05
Vwf	von Willebrand factor homolog	−1.83	9.95×10^{-4}	−1.78	1.77×10^{-3}	−1.03	0.89
Sfrp2	Secreted frizzled-related protein 2	−1.91	1.07×10^{-3}	−1.37	0.108	−1.39	0.10
Ccl11	Chemokine (C-C motif) ligand 11	−1.58	1.43×10^{-3}	1.09	0.556	**−1.73**	**4.37×10^{-4}**
Bst1	Bone marrow stromal cell antigen 1	−1.74	2.64×10^{-3}	−1.45	0.034	−1.19	0.33
Cntfr	Ciliary neurotrophic factor receptor	−1.57	2.80×10^{-3}	−1.77	1.26×10^{-4}	1.13	0.41
Ptgfr	Prostaglandin F receptor	−1.55	3.03×10^{-3}	−1.15	0.413	−1.35	0.08
Inmt	Indolethylamine *N*-methyltransferase	−1.66	3.84×10^{-3}	−1.46	0.021	**−2.13**	**2.73×10^{-16}**
Aqp4	Aquaporin 4	−1.51	4.77×10^{-3}	−1.39	0.069	−1.08	0.66
Dlg2	Disks, large homolog 2 (Drosophila)	−1.51	5.23×10^{-3}	−1.00	0.974	−1.49	0.01
Tmem119	Transmembrane protein 119	−1.51	7.18×10^{-3}	−1.13	0.426	−1.33	0.07
Comp	Cartilage oligomeric matrix protein	−1.61	7.24×10^{-3}	1.37	0.180	**−2.20**	**9.30×10^{-4}**
Tmem108	Transmembrane protein 108	−1.56	8.66×10^{-3}	−1.96	2.85×10^{-3}	1.25	0.32
Gm14391	Predicted gene 14391	−2.25	9.13×10^{-3}	1.30	0.386	**−2.91**	**5.62×10^{-4}**
Tnfrsf25	Tumor necrosis factor receptor superfamily, member 25	−1.66	9.63×10^{-3}	−1.52	3.76×10^{-2}	−1.09	0.68
Bmx	BMX nonreceptor tyrosine kinase	−1.69	1.24×10^{-2}	−1.14	0.457	−1.47	0.04
Six1	Sine oculis-related homeobox 1	−1.67	1.27×10^{-2}	−4.58	1.94×10^{-10}	2.74	1.96×10^{-5}
Ism1	Isthmin 1 homolog (zebrafish)	−1.59	1.66×10^{-2}	−2.16	1.83×10^{-4}	1.37	0.13
Sall1	Sal-like 1 (Drosophila)	−1.81	1.75×10^{-2}	−2.07	2.56×10^{-2}	1.14	0.68
Ddit4l	DNA damage inducible transcript 4-like	−1.51	1.89×10^{-2}	−1.27	0.113	−1.18	0.27
Hhipl1	Hedgehog interacting protein-like 1	−1.55	1.90×10^{-2}	−1.05	0.769	−1.48	0.02
Clvs1	clavesin 1	−1.75	1.93×10^{-2}	−1.68	2.07×10^{-2}	−1.04	0.87
310015D24Rik	RIKEN cDNA 2310015D24 gene	−1.52	2.08×10^{-2}	−1.02	0.894	−1.48	0.02
Ccl19	Chemokine (C-C motif) ligand 19	−1.72	2.35×10^{-2}	−1.23	0.325	−1.39	0.13
Gdf6	Growth differentiation factor 6	−1.62	2.43×10^{-2}	−1.55	3.63×10^{-2}	−1.04	0.86
Kif1a	Kinesin family member 1A	−1.57	2.56×10^{-2}	−1.47	0.044	−1.07	0.73
Adam33	A disintegrin and metallopeptidase domain 33	−1.63	2.90×10^{-2}	−1.45	0.090	−1.13	0.60
Pamr1	Peptidase domain containing associated with muscle regeneration 1	−1.59	3.28×10^{-2}	1.07	0.713	**−1.71**	**6.92×10^{-3}**
Neb	Nebulin	−1.71	3.64×10^{-2}	−1.01	0.962	−1.68	0.07
Enpp6	Ectonucleotide pyrophosphatase/phosphodiesterase 6	−1.51	3.78×10^{-2}	−1.64	2.43×10^{-2}	1.09	0.69
Gm3776	Predicted gene 3776	−1.58	3.95×10^{-2}	1.35	0.149	**−2.12**	**3.49×10^{-4}**

Continued

Table 3.—*Continued*

Gene Symbol	Name	Saline vs. E-cigarette (2.4%) Fold change	Saline vs. E-cigarette (2.4%) *P* value	Saline vs. E-cigarette (0%) Fold change	Saline vs. E-cigarette (0%) *P* value	E-cigarette (0%) vs. E-cigarette (2.4%) Fold change	E-cigarette (0%) vs. E-cigarette (2.4%) *P* value
Nmb	Neuromedin B	−1.54	4.01×10^{-2}	1.02	0.907	−1.31	0.12
Rorb	RAR-related orphan receptor-β	−1.50	4.10×10^{-2}	−1.22	0.252	−1.23	0.25
Ahsg	α2-HS-glycoprotein	−1.64	4.97×10^{-2}	−1.91	3.66×10^{-2}	1.17	0.62

Saline vs. electronic cigarette (e-cigarette) (2.4%) columns show the fold changes and *P* value of the differentially downregulated genes between saline aerosol and e-cigarette (2.4%). Saline vs. e-cigarette (0%) columns show all the changes between saline and e-cigarette (0%) for the listed genes. In the saline vs. e-cigarette (0%) columns, the changes underlined are similar to the saline vs. e-cigarette (2.4%) column. The similar downregulation in gene expression (underlined) suggests that the changes in the saline vs. e-cigarette (2.4%) column are nicotine independent for the associated gene. E-cigarette (0%) vs. e-cigarette (2.4%) columns show all the changes between e-cigarette (0%) and e-cigarette (2.4%) in the listed genes. In the e-cigarette (0%) vs. e-cigarette (2.4%) columns, the changes marked in boldface are similar to the saline vs. e-cigarette (2.4%) column. These similar changes in gene expression (in boldface) suggest that changes in the saline vs. e-cigarette (2.4%) column are dependent of nicotine for the associated genes. Genes showing altered expression with $P < 0.05$, >1.5-fold changes in akin direction, were considered differentially expressed in a similar way.

well as vascular inflammation (9). Impairment of systolic function often appears early in the course of heart disease. For example, impaired left ventricular dysfunction is already present in patients with metabolic syndrome (42). ApoE$^{-/-}$ mice exposed to e-cigarette (2.4%) show a marked decrease in systolic function without changes in diastolic parameters. Heart size and heart/body ratio did not change. We did not observe development of systolic dysfunction in mice exposed to e-cigarette (0%). Therefore, nicotine is the main origin of the induction of systolic dysfunction in this model. Altogether, these data suggest an early stage of cardiac dysfunction before fibrosis and heart failure develops.

ApoE$^{-/-}$ mice were euthanized immediately after the first detection of systolic dysfunction since we desired to understand the mechanisms underlying the onset of e-cigarette (2.4%)-induced cardiac dysfunction without the plethora of changes produced by cardiac remodeling (17). To distinguish different etiologies of cardiac dysfunction by their gene expression fingerprint, we performed an RNA-seq analysis. IPA analysis revealed dysregulation in gene clusters of inflammatory, circadian rhythm, and leukocyte extravasation signaling. The mechanism triggering these cardiac alterations appears to be the proinflammatory environment promoted by FFA release induced by nicotine. For instance, we observed increases of COL5A3 and TNFRSF12A. COL5A3 is increased in inflammatory processes (53) including atherosclerotic lesions (59) and extracellular matrix remodeling (53). TNFRSF12A mRNA level is increased in an ROS-induced heart failure model (61). Consistent with our data, Per2 knockout mice have an increased inflammatory response in the heart (15). Interestingly, Per2 and Per3 mRNA expressions are altered in streptozotocin-induced diabetic rats, associating these changes either directly or indirectly with changes in insulin levels (83). Additionally, an increased leukocyte extravasation signaling has been associated with detrimental effects in atherosclerosis and cardiac dysfunction (77). For example, RNA-seq analysis shows an increase in expression of Ras guanyl-releasing protein 1, which is necessary for the angiotensin II-induced cardiac dysfunction (49). We observed increased levels of SCD1 mRNA, which is associated with decreased contractile function in obese hearts (24). We did not observe any changes in collagen in type I/collagen type III ratio mRNA, which is increased in fibrosis. In accordance, fibrosis is a late consequence of cardiac dysfunction in a diet-induced model of cardiac dysfunction (28) that was not present in the 12-wk exposure period of these experiments.

Intriguingly, we also found 226 genes that were differentially expressed between saline aerosol and non-nicotine e-cigarette (0%) exposed hearts. Furthermore, 29 differentially expressed genes were similarly expressed in the nicotine e-cigarette (2.4%)-treated group when compared with non-nicotine e-cigarette (0%) or saline-exposed groups (Tables 2 and 3, underlined). Thus, although our data show that e-cigarettes only in the presence of nicotine (2.4%) have detrimental effects on cardiac function, we cannot rule out the possibility that other substances in the e-cigarettes other than nicotine may

Table 4. *Canonical pathways tested by IPA*

IPA Category	Gene Symbol	Gene Name
Inflammatory signaling	CCR2	Chemokine (C-C motif) receptor 2
	COL5A3	Collagen, type V, α3
	TNFRSF12A	Tumor necrosis factor receptor superfamily, member 12a
	CCL11	Chemokine (C-C motif) ligand 11
	SELE	Selectin E
Circadian rhythm signaling	PER3	Period circadian regulator 3
	PER2	Period circadian regulator 2
	GRIN2C	Glutamate receptor, ionotropic, NMDA2C (ε3)
Leukocyte extravasation signaling	ITGAL	Integrin αL
	BMX	BMX nonreceptor tyrosine kinase
	TIMP4	Tissue inhibitor of metalloproteinase 4
	RASGRP1	RAS guanyl-releasing protein 1

Most representative canonical pathways deregulated in mice exposed to electronic cigarettes (2.4%). We have added blue arrows pointing to genes associated with the IPA analysis in Fig. 2*A*. IPA, Ingenuity Pathway Analysis.

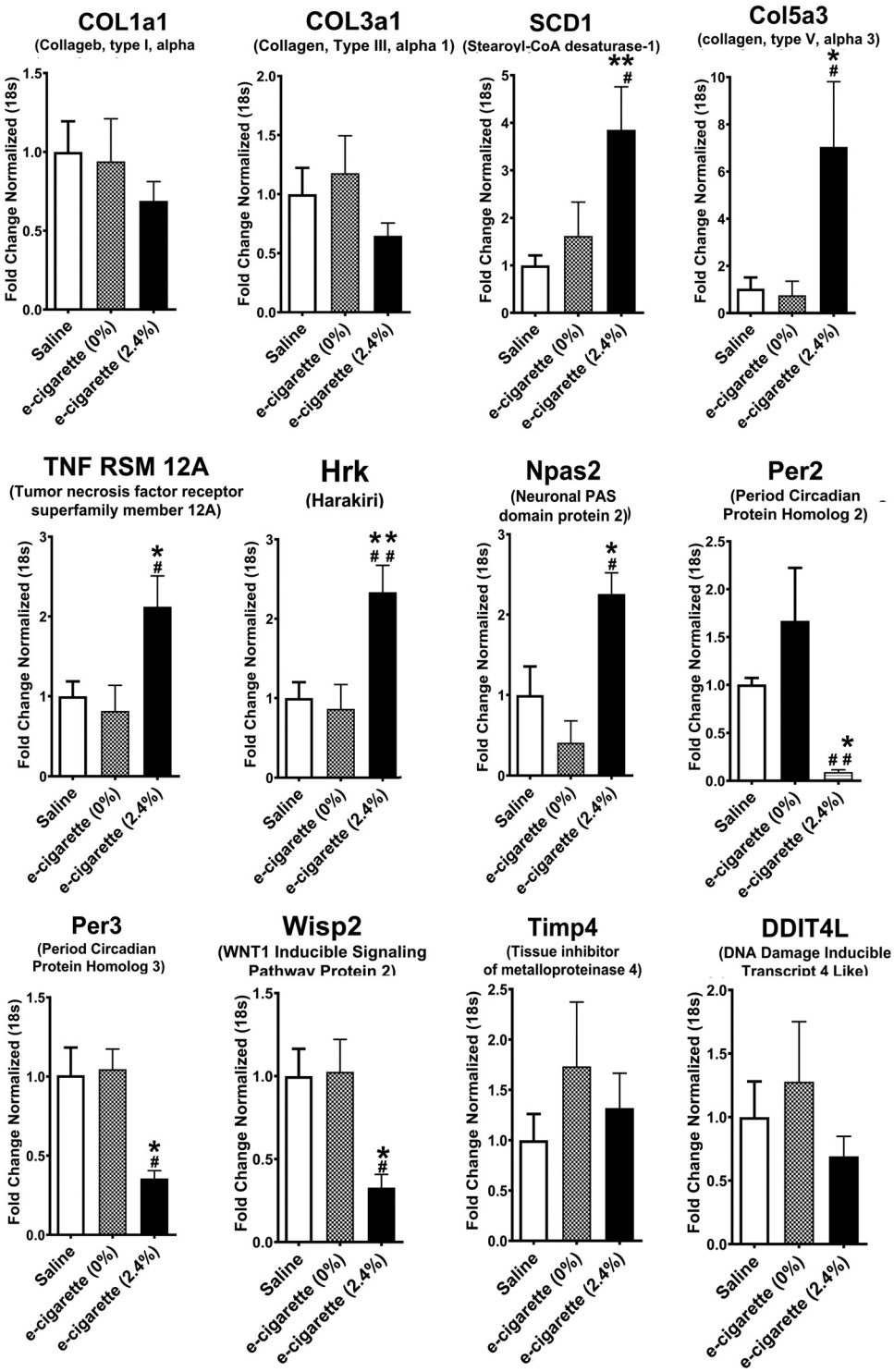

Fig. 3. Validation of relative expression of genes obtained from RNA-seq by quantitative PCR. Relative quantification normalized to 18s. [$n = 5$ per group; saline vs. electronic cigarette (e-cigarette) (2.4%), $^{*}P < 0.05$, $^{**}P < 0.01$; e-cigarette (0%) vs. e-cigarette (2.4%), $\#P < 0.05$, $\#\#P < 0.01$]. COL1a1, collagen type I α1; COL3a1, collagen type III α1; Col5a3, collagen type V α3; Hrk, harakiri; Npas2, neuronal PAS domain protein 2; Per2, period circadian protein homolog 2; Per3, period circadian protein homolog 3; Ddit4m, DNA damage inducible transcript 4 like; SCD1, stearoyl-CoA desaturase-1; Timp4, tissue inhibitor of metalloproteinase 4; TNF RSM 12A, Tumor necrosis factor receptor superfamily member 12A; Wisp2, WNT1 inducible signaling pathway protein 2.

have some detrimental health effects. This nicotine-independent transcriptomic effect clearly merits further investigation. We also observed 241 genes that were differentially expressed between e-cigarettes with (2.4%) and without (0%) nicotine. There were 40 genes showing the similar changes caused by nicotine e-cigarette (2.4%) compared with non-nicotine e-cigarette (0%) or saline (Tables 2 and 3, in boldface).

We observed an increase in serum FFA levels in mice treated with e-cigarette (2.4%). FFAs released into circulation have been extensively studied in their contribution to the induction of metabolic changes that lead to metabolic syndrome and adverse cardiovascular outcomes (56). Inhibition of adipose tissue lipolysis using acipimox-reduced nicotine plus high-fat diet (HFD)-induced hepatic steatosis (23), a common antecedent of metabolic syndrome. FFA generation is likely one of the key elements in ectopic lipid accumulation, lipotoxicity, mitochondrial dysfunction (18, 33, 35), and cardiomyopathy (14, 17). In e-cigarette (2.4%)-treated mice, we observed

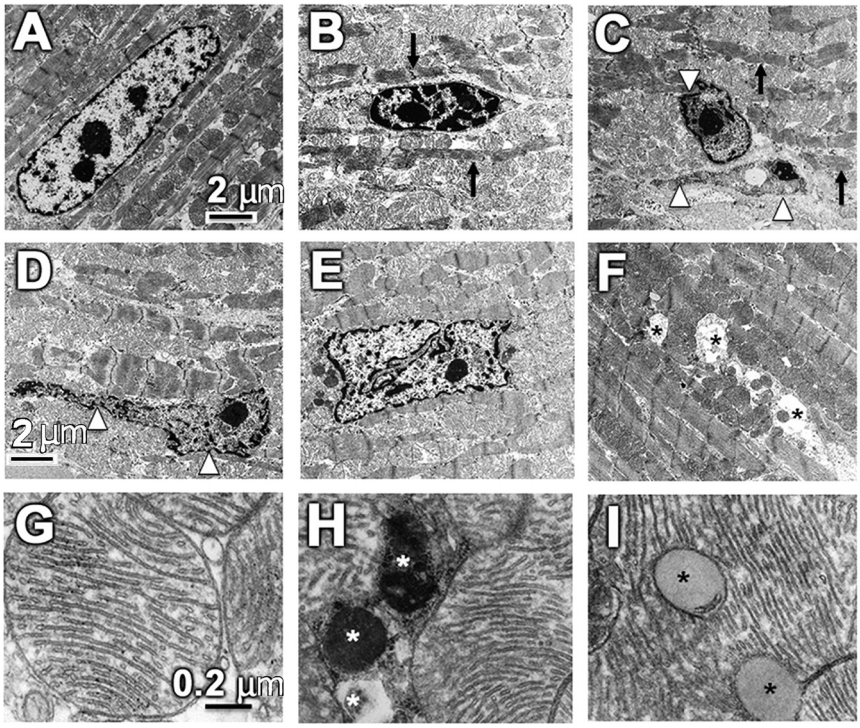

Fig. 4. Electronic cigarette (e-cigarette) (2.4%) causes cardiomyocyte (CM) nuclear and myofibrillar abnormalities. *A–F*: representative transmission electron microscopy (TEM) images of left ventricles from apolipoprotein-E knockout mice on a Western diet exposed to e-cigarette (2.4%). *A*: representative CMs from mice exposed to saline aerosol showing normal myofibrillar architecture and sarcomeric pattern with a normal nucleus and abundant mitochondria. *B–F*: nuclear and cytoplasmic abnormalities observed in e-cigarette (2.4%)-treated mice. The most prominent nuclear abnormalities include shrunken nuclei, showing characteristic of apoptosis, and nuclei with extensively convoluted nuclear membrane (white arrowhead). The most striking cytoplasmic abnormalities include myofibrillar derangement, thinning, and destruction (black arrow). Scale bar = 2 μm. *G–I*: representative higher magnification of TEM images of left ventricles. *G*: normal mitochondrial ultrastructure observed in mice exposed to saline aerosol. *H* and *I*: TEM images show mitophagy (white asterisks) and intramyocardial lipid accumulation (black asterisks) in e-cigarette (2.4%)-treated mice. Scale bar = 0.2 μm.

increased intramyocardial lipid accumulation and mitophagy abnormalities by ultrastructural analysis. FFAs can increase mitochondrial generation of ROS, and increased ROS by FFA-induced mitochondrial dysfunction has been postulated as a major mechanism of metabolic syndrome (20, 71).

Of note, in this study, we elect to use ApoE$^{-/-}$ mice to study the effects of e-cigarettes (2.4%) on cardiovascular function and pathophysiology, as these mice on a WD (40% calories derived from fat) as opposed to an HFD with 60% of calories derived from fat, are a widely used murine model of atherosclerosis (65) and have been used to study the cardiovascular effects of conventional cigarettes (50). In this context, it is worth noting that in an earlier report, we found no differences in plasma FAA levels in C57BL/6 mice on a normal diet in the absence of the presence of nicotine (76). Although an HFD alone, as opposed to a WD, resulted in a modest increase in plasma FFA levels, nicotine, when combined with an HFD, caused a striking increase in plasma FFA levels (82). This is also consistent with a pervious study showing that nicotine, when combined an HFD, promotes lipolysis and increases in serum FAA levels (82). We observed a tendency of nicotine to decrease ApoE$^{-/-}$ body weight that was not statistically significant. Since nicotine has been reported to reduce body weight gain in HFD-fed mice (23, 55, 76), a significant effect of nicotine on body weight may not be ruled out using more mice with a different experimental design.

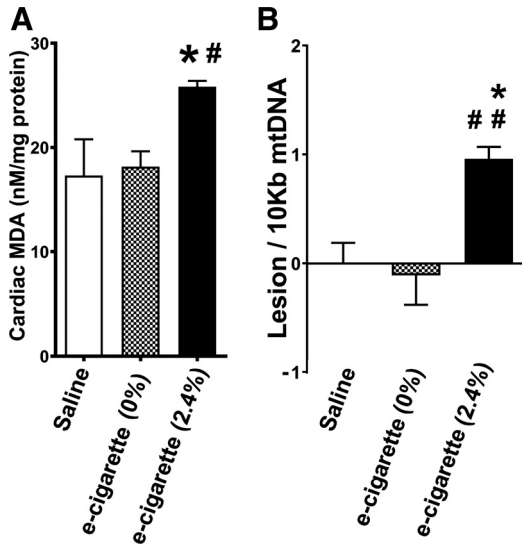

Fig. 5. Electronic cigarette (e-cigarette) (2.4%) effects on reactive oxygen species induction and mitochondrial dysfunction. *A*: malondialdehyde (MDA) generation associated with e-cigarette (2.4%) exposure. *B*: mtDNA lesions in cardiac cells ($n = 5$ per group; saline vs. e-cigarette (2.4%), $^{*}P < 0.05$, $^{**}P < 0.01$; e-cigarette (0%) vs. e-cigarette (2.4%), $\#P < 0.05$, $\#\#P < 0.01$).

E-cigarettes produce oxidative stress in both in vitro and in vivo models (47, 81). Here, we show a proinflammatory cardiac phenotype with increased MDA and mtDNA mutation levels in mice exposed to e-cigarette (2.4%). MDA is used as a marker of increased ROS generation, and MDA levels have been applied as an indicator of lipid peroxidation and oxidative stress in a number of cardiovascular disease models (34). Smokers show increased levels of mtDNA damage (6), humans and mouse models of metabolic disease also have increased cardiac mtDNA mutations (32), and we observed increased levels of mtDNA mutations in mice treated with e-cigarettes (2.4%). The mtDNA mutations can lead to mitochondrial dysfunction and insufficient energy production of cardiac cells (45).

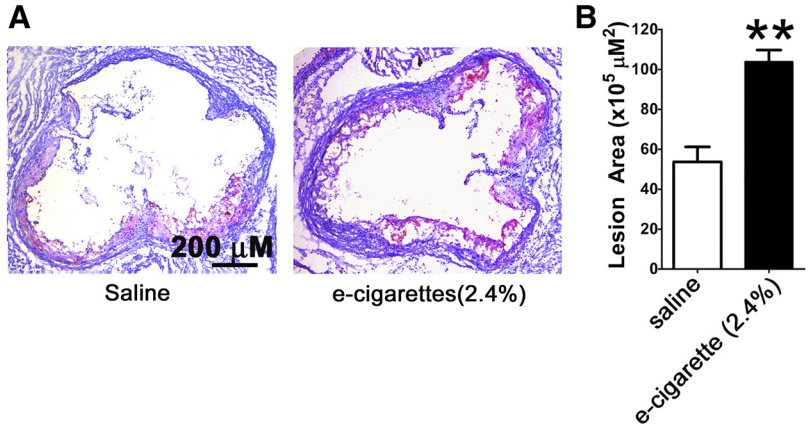

Fig. 6. Electronic cigarette (e-cigarette) (2.4%) induces atherosclerotic lesion formation. *A*: Oil Red O counterstained with hematoxylin and fast green for visualization. Scale bar = 200 μm. *B*: atherosclerotic lesions quantified with Image-Pro Plus ($n = 5$ per group; $^{**}P < 0.01$).

We show that e-cigarettes (2.4%) lead to plaque formation in the aortic root of ApoE$^{-/-}$ mice. Although nicotine-induced release of FFAs from adipocytes has a role in communication between adipocyte tissue and the vascular walls (2, 26), nicotine also accelerates atherosclerosis by direct activation of nicotinic receptors in endothelial, vascular smooth muscle, and mast cells (44, 80). Further experiments are needed to define the precise contribution of these mechanisms in the atherosclerotic phenotype observed in mice exposed to nicotine e-cigarettes.

E-cigarettes are associated with increased risk of myocardial infarction (3). ROS production correlates with development of atherosclerosis, and cardiomyopathy. Increased levels of ROS are a common characteristic of the development of atherosclerosis and cardiomyopathy (16, 81). Endothelial cells play a critical role in maintaining the integrity of the vessel wall, and in healthy voluntaries, 10 puffs of e-cigarettes produce an increase of endothelial progenitor cells and circulating microvesicles, which are markers of endothelial dysfunction (4). In the current study, we show that e-cigarettes (2.4%) exacerbate spontaneous plaque formation in the aortic root of ApoE$^{-/-}$ mice. Further experiments are planned with e-cigarette (0%) to confirm that the nicotine in e-cigarettes leads to the atherogenic phenotype. Our data provide evidence of the proatherosclerotic property of nicotine e-cigarettes. Further experiments are needed to define the precise contribution of mechanisms involved in the atherosclerotic phenotype observed in mice exposed to e-cigarettes (2.4%).

This study is primarily focused to determine the detrimental cardiac and atherosclerotic effects of e-cigarettes, as these products are relatively new and studies are needed to determine their long-term detrimental effects, some of which may be similar to the long-term detrimental effects of nicotine. Our results demonstrate adverse effects of e-cigarettes on cardiac structure and function in mice. The results of the present study also confirm and extend our earlier study (75) in which we demonstrated that intraperitoneal injections of nicotine generate oxidative stress and trigger CM apoptosis, which has been implicated as a potential mechanism in the development of cardiomyopathy and heart failure (46, 54) in obese mice. Available evidence also suggests that nicotine delivered via mini osmotic pump can exacerbate angiotensin II-induced cardiovascular remodeling in a mouse model of systemic hypertension (19). Taken together, these results suggest that nicotine is most likely responsible for the observed cardiac effects. However, further work will be needed to understand if nicotine delivered by another route, such as gums or transdermal patch, yields similar effects.

The strengths of our study include using a novel e-cigarette delivery technology mimicking human vaping and using a leading brand of e-cigarettes that achieved serum cotinine levels in the range found in heavy smokers. E-cigarettes (2.4%) also caused CMs ultrastructural abnormalities indicative of cardiomyopathy and contractile dysfunction. The ultrastructural changes in CMs are structural manifestations of altered cardiac LV function in response to the e-cigarettes (2.4%) exposure. We used a 12-wk treatment period that did not lead to hypertrophy; a longer period may lead to a more severe phenotype with ventricular hypertrophy and fibrosis (23).

In conclusion, nicotine e-cigarettes (2.4%) induce a proinflammatory phenotype associated with cardiac dysfunction and atherogenesis, in which ROS levels are abnormally increased and an increase in mtDNA mutations occur. Our results highlight multiple detrimental effects of nicotine e-cigarettes on the cardiovascular system. Increased ROS and impaired mitochondrial function and its targets likely contribute to the etiology of cardiovascular system dysfunction. Our findings question the claim that nicotine e-cigarettes are safe.

GRANTS

This work was supported by Diversity-Promoting Institution Drug Abuse Research Program Grant R24DA017298; a pilot project grant and vouchers from Accelerating Excellence in Translational Science Grant 5U54MD007598 from the National Institutes of Health (NIH); and a California Tobacco-Related Disease Research Program Grant 251P003. Y. Liu is supported by NIH Grant SC1-DK-104821. J. Espinoza-Derout has been supported in part by National Institute on Minority Health and Health Disparities Grant S21-MD000103.

DISCLOSURES

No conflicts of interest, financial or otherwise, are declared by the authors.

AUTHOR CONTRIBUTIONS

J.E.-D., X.M.S., A.P.S.-H., and T.C.F. conceived and designed research; J.E.-D., K.M.H., M.C.J., C.S., D.L.L., Z.S., and Y.L. performed experiments; J.E.-D., X.M.S., S.S., and K.P.R. analyzed data; J.E.-D., K.M.H., X.M.S., Z.S., Y.L., K.P.R., A.P.S.-H., and T.C.F. interpreted results of experiments; J.E.-D. prepared figures; J.E.-D., K.M.H., X.M.S., and T.C.F. drafted manuscript; J.E.-D., X.M.S., N.M., A.P.S.-H., and T.C.F. edited and revised manuscript; T.C.F. approved final version of manuscript.

REFERENCES

1. **Aickin M, Gensler H.** Adjusting for multiple testing when reporting research results: the Bonferroni vs Holm methods. *Am J Public Health* 86: 726–728, 1996. doi:10.2105/AJPH.86.5.726.
2. **Akoumianakis I, Antoniades C.** The interplay between adipose tissue and the cardiovascular system: is fat always bad? *Cardiovasc Res* 113: 999–1008, 2017. doi:10.1093/cvr/cvx111.
3. **Alzahrani T, Pena I, Temesgen N, Glantz SA.** Association between electronic cigarette use and myocardial infarction. *Am J Prev Med* 55: 455–461, 2018. doi:10.1016/j.amepre.2018.05.004.
4. **Antoniewicz L, Bosson JA, Kuhl J, Abdel-Halim SM, Kiessling A, Mobarrez F, Lundbäck M.** Electronic cigarettes increase endothelial progenitor cells in the blood of healthy volunteers. *Atherosclerosis* 255: 179–185, 2016. doi:10.1016/j.atherosclerosis.2016.09.064.
5. **Baglione J, Smith JD.** Quantitative assay for mouse atherosclerosis in the aortic root. *Methods Mol Med* 129: 83–95, 2006. doi:10.1385/1-59745-213-0:83.
6. **Ballinger SW, Bouder TG, Davis GS, Judice SA, Nicklas JA, Albertini RJ.** Mitochondrial genome damage associated with cigarette smoking. *Cancer Res* 56: 5692–5697, 1996.
7. **Barrera-Vilarmau S, Obregón P, de Alba E.** Intrinsic order and disorder in the bcl-2 member harakiri: insights into its proapoptotic activity. *PLoS One* 6: e21413, 2011. doi:10.1371/journal.pone.0021413.
8. **Benowitz NL, Burbank AD.** Cardiovascular toxicity of nicotine: Implications for electronic cigarette use. *Trends Cardiovasc Med* 26: 515–523, 2016. doi:10.1016/j.tcm.2016.03.001.
9. **Benowitz NL, Fraiman JB.** Cardiovascular effects of electronic cigarettes. *Nat Rev Cardiol* 14: 447–456, 2017. doi:10.1038/nrcardio.2017.36.
10. **Benowitz NL, Gourlay SG.** Cardiovascular toxicity of nicotine: implications for nicotine replacement therapy. *J Am Coll Cardiol* 29: 1422–1431, 1997. doi:10.1016/S0735-1097(97)00079-X.
11. **Benowitz NL, Zevin S, Jacob P 3rd.** Sources of variability in nicotine and cotinine levels with use of nicotine nasal spray, transdermal nicotine, and cigarette smoking. *Br J Clin Pharmacol* 43: 259–267, 1997. doi:10.1111/j.1365-2125.1997.00566.x.
12. **Bhatnagar A, Whitsel LP, Ribisl KM, Bullen C, Chaloupka F, Piano MR, Robertson RM, McAuley T, Goff D, Benowitz N; American Heart Association Advocacy Coordinating Committee, Council on Cardiovascular and Stroke Nursing, Council on Clinical Cardiology, and Council on Quality of Care and Outcomes Research.** Electronic cigarettes: a policy statement from the American Heart Association. *Circulation* 130: 1418–1436, 2014. doi:10.1161/CIR.0000000000000107.
13. **Bitzer ZT, Goel R, Reilly SM, Foulds J, Muscat J, Elias RJ, Richie JP Jr.** Effects of solvent and temperature on free radical formation in electronic cigarette aerosols. *Chem Res Toxicol* 31: 4–12, 2018. doi:10.1021/acs.chemrestox.7b00116.
14. **Boden G.** Obesity, insulin resistance and free fatty acids. *Curr Opin Endocrinol Diabetes Obes* 18: 139–143, 2011. doi:10.1097/MED.0b013e3283444b09.
15. **Bonney S, Kominsky D, Brodsky K, Eltzschig H, Walker L, Eckle T.** Cardiac Per2 functions as novel link between fatty acid metabolism and myocardial inflammation during ischemia and reperfusion injury of the heart. *PLoS One* 8: e71493, 2013. doi:10.1371/journal.pone.0071493.
16. **Brookheart RT, Michel CI, Schaffer JE.** As a matter of fat. *Cell Metab* 10: 9–12, 2009. doi:10.1016/j.cmet.2009.03.011.
17. **Chong CR, Clarke K, Levelt E.** Metabolic remodeling in diabetic cardiomyopathy. *Cardiovasc Res* 113: 422–430, 2017. doi:10.1093/cvr/cvx018.
18. **Chow J, Rahman J, Achermann JC, Dattani MT, Rahman S.** Mitochondrial disease and endocrine dysfunction. *Nat Rev Endocrinol* 13: 92–104, 2017. doi:10.1038/nrendo.2016.151.
19. **Colombo ES, Davis J, Makvandi M, Aragon M, Lucas SN, Paffett ML, Campen MJ.** Effects of nicotine on cardiovascular remodeling in a mouse model of systemic hypertension. *Cardiovasc Toxicol* 13: 364–369, 2013. doi:10.1007/s12012-013-9217-z.
20. **Daniele G, Eldor R, Merovci A, Clarke GD, Xiong J, Tripathy D, Taranova A, Abdul-Ghani M, DeFronzo RA.** Chronic reduction of plasma free fatty acid improves mitochondrial function and whole-body insulin sensitivity in obese and type 2 diabetic individuals. *Diabetes* 63: 2812–2820, 2014. doi:10.2337/db13-1130.
21. **Durgan DJ, Young ME.** The cardiomyocyte circadian clock: emerging roles in health and disease. *Circ Res* 106: 647–658, 2010. doi:10.1161/CIRCRESAHA.109.209957.
22. **Fowler PA, Childs AJ, Courant F, MacKenzie A, Rhind SM, Antignac JP, Le Bizec B, Filis P, Evans F, Flannigan S, Maheshwari A, Bhattacharya S, Monteiro A, Anderson RA, O'Shaughnessy PJ.** In utero exposure to cigarette smoke dysregulates human fetal ovarian developmental signalling. *Hum Reprod* 29: 1471–1489, 2014. doi:10.1093/humrep/deu117.
23. **Friedman TC, Sinha-Hikim I, Parveen M, Najjar SM, Liu Y, Mangubat M, Shin CS, Lyzlov A, Ivey R, Shaheen M, French SW, Sinha-Hikim AP.** Additive effects of nicotine and high-fat diet on hepatic steatosis in male mice. *Endocrinology* 153: 5809–5820, 2012. doi:10.1210/en.2012-1750.
24. **Ge F, Hu C, Hyodo E, Arai K, Zhou S, Lobdell H IV, Walewski JL, Homma S, Berk PD.** Cardiomyocyte triglyceride accumulation and reduced ventricular function in mice with obesity reflect increased long chain fatty acid uptake and de novo fatty acid synthesis. *J Obes* 2012: 1–12, 2012. doi:10.1155/2012/205648.
25. **Getz GS, Reardon CA.** Animal models of atherosclerosis. *Arterioscler Thromb Vasc Biol* 32: 1104–1115, 2012. doi:10.1161/ATVBAHA.111.237693.
26. **Ghosh A, Gao L, Thakur A, Siu PM, Lai CW.** Role of free fatty acids in endothelial dysfunction. *J Biomed Sci* 24: 50, 2017. doi:10.1186/s12929-017-0357-5.
27. **Glantz SA, Bareham DW.** E-cigarettes: use, effects on smoking, risks, and policy implications. *Annu Rev Public Health* 39: 215–235, 2018. doi:10.1146/annurev-publhealth-040617-013757.
28. **Gonçalves N, Silva AF, Rodrigues PG, Correia E, Moura C, Eloy C, Roncon-Albuquerque R Jr, Falcão-Pires I, Leite-Moreira AF.** Early cardiac changes induced by a hypercaloric Western-type diet in "subclinical" obesity. *Am J Physiol Heart Circ Physiol* 310: H655–H666, 2016. doi:10.1152/ajpheart.00684.2015.
29. **Gooley JJ, Chua EC.** Diurnal regulation of lipid metabolism and applications of circadian lipidomics. *J Genet Genomics* 41: 231–250, 2014. doi:10.1016/j.jgg.2014.04.001.
30. **Hajek P, Phillips-Waller A, Przulj D, Pesola F, Myers Smith K, Bisal N, Li J, Parrott S, Sasieni P, Dawkins L, Ross L, Goniewicz M, Wu Q, McRobbie HJ.** A randomized trial of e-cigarettes versus nicotine-replacement therapy. *N Engl J Med* 380: 629–637, 2019. doi:10.1056/NEJMoa1808779.
31. **Herder C, Schamarek I, Nowotny B, Carstensen-Kirberg M, Straßburger K, Nowotny P, Kannenberg JM, Strom A, Püttgen S, Müssig K, Szendroedi J, Roden M, Ziegler D; German Diabetes Study Group.** Inflammatory markers are associated with cardiac autonomic dysfunction in recent-onset type 2 diabetes. *Heart* 103: 63–70, 2017. doi:10.1136/heartjnl-2015-309181.
32. **Herst PM, Rowe MR, Carson GM, Berridge MV.** Functional mitochondria in health and disease. *Front Endocrinol (Lausanne)* 8: 296, 2017. doi:10.3389/fendo.2017.00296.
33. **Hirabara SM, Curi R, Maechler P.** Saturated fatty acid-induced insulin resistance is associated with mitochondrial dysfunction in skeletal muscle cells. *J Cell Physiol* 222: 187–194, 2010. doi:10.1002/jcp.21936.
34. **Ho E, Karimi Galougahi K, Liu CC, Bhindi R, Figtree GA.** Biological markers of oxidative stress: Applications to cardiovascular research and practice. *Redox Biol* 1: 483–491, 2013. doi:10.1016/j.redox.2013.07.006.
35. **Hoeks J, van Herpen NA, Mensink M, Moonen-Kornips E, van Beurden D, Hesselink MK, Schrauwen P.** Prolonged fasting identifies skeletal muscle mitochondrial dysfunction as consequence rather than cause of human insulin resistance. *Diabetes* 59: 2117–2125, 2010. doi:10.2337/db10-0519.
36. **Hukkanen J, Jacob P 3rd, Benowitz NL.** Metabolism and disposition kinetics of nicotine. *Pharmacol Rev* 57: 79–115, 2005. doi:10.1124/pr.57.1.3.
37. **Husari A, Shihadeh A, Talih S, Hashem Y, El Sabban M, Zaatari G.** Acute exposure to electronic and combustible cigarette aerosols: effects in an animal model and in human alveolar cells. *Nicotine Tob Res* 18: 613–619, 2016. doi:10.1093/ntr/ntv169.
38. **Inohara N, Ding L, Chen S, Núñez G.** *harakiri*, a novel regulator of cell death, encodes a protein that activates apoptosis and interacts selectively with survival-promoting proteins Bcl-2 and Bcl-X_L. *EMBO J* 16: 1686–1694, 1997. doi:10.1093/emboj/16.7.1686.
39. **Jacob P 3rd, Yu L, Duan M, Ramos L, Yturralde O, Benowitz NL.** Determination of the nicotine metabolites cotinine and trans-3′-hydroxycotinine in biologic fluids of smokers and non-smokers using liquid chromatography-tandem mass spectrometry: biomarkers for tobacco smoke exposure and for phenotyping cytochrome P450 2A6 activity. *J*

Chromatogr B Analyt Technol Biomed Life Sci 879: 267–276, 2011. doi:10.1016/j.jchromb.2010.12.012.

40. **Koskivirta I, Kassiri Z, Rahkonen O, Kiviranta R, Oudit GY, McKee TD, Kytö V, Saraste A, Jokinen E, Liu PP, Vuorio E, Khokha R.** Mice with tissue inhibitor of metalloproteinases 4 (Timp4) deletion succumb to induced myocardial infarction but not to cardiac pressure overload. *J Biol Chem* 285: 24487–24493, 2010. doi:10.1074/jbc.M110.136820.
41. **Kristjansson AL, Mann MJ, Smith ML.** Prevalence of substance use among middle school-aged e-cigarette users compared with cigarette smokers, nonusers, and dual users: Implications for primary prevention. *Subst Abus* 38: 473–476, 2017. doi:10.1080/08897077.2017.1343218.
42. **La Carrubba S, Todaro MC, Zito C, Antonini-Canterin F, Monte IP, Caso P, Colonna P, de Gregorio C, Pezzano A, Benedetto F, Salvo GD, Carerj S, Bello VD.** Asymptomatic left ventricular dysfunction and metabolic syndrome: results from an Italian multicenter study. *J Cardiovasc Echogr* 23: 96–101, 2013. doi:10.4103/2211-4122.127410.
43. **Langmead B, Salzberg SL.** Fast gapped-read alignment with Bowtie 2. *Nat Methods* 9: 357–359, 2012. doi:10.1038/nmeth.1923.
44. **Lee J, Cooke JP.** The role of nicotine in the pathogenesis of atherosclerosis. *Atherosclerosis* 215: 281–283, 2011. doi:10.1016/j.atherosclerosis.2011.01.003.
45. **Lee SR, Kim N, Noh YH, Xu Z, Ko KS, Rhee BD, Han J.** Mitochondrial DNA, mitochondrial dysfunction, and cardiac manifestations. *Front Biosci* 22: 1177–1194, 2017. doi:10.2741/4541.
46. **Lee Y, Gustafsson AB.** Role of apoptosis in cardiovascular disease. *Apoptosis* 14: 536–548, 2009. doi:10.1007/s10495-008-0302-x.
47. **Lerner CA, Sundar IK, Yao H, Gerloff J, Ossip DJ, McIntosh S, Robinson R, Rahman I.** Vapors produced by electronic cigarettes and e-juices with flavorings induce toxicity, oxidative stress, and inflammatory response in lung epithelial cells and in mouse lung. *PLoS One* 10: e0116732, 2015. doi:10.1371/journal.pone.0116732.
48. **Li B, Dewey CN.** RSEM: accurate transcript quantification from RNA-Seq data with or without a reference genome. *BMC Bioinformatics* 12: 323, 2011. doi:10.1186/1471-2105-12-323.
49. **Li L, Fan D, Wang C, Wang JY, Cui XB, Wu D, Zhou Y, Wu LL.** Angiotensin II increases periostin expression via Ras/p38 MAPK/CREB and ERK1/2/TGF-β1 pathways in cardiac fibroblasts. *Cardiovasc Res* 91: 80–89, 2011. doi:10.1093/cvr/cvr067.
50. **Lo Sasso G, Schlage WK, Boué S, Veljkovic E, Peitsch MC, Hoeng J.** The Apoe(-/-) mouse model: a suitable model to study cardiovascular and respiratory diseases in the context of cigarette smoke exposure and harm reduction. *J Transl Med* 14: 146, 2016. doi:10.1186/s12967-016-0901-1.
51. **Lukyanenko V, Chikando A, Lederer WJ.** Mitochondria in cardiomyocyte Ca2+ signaling. *Int J Biochem Cell Biol* 41: 1957–1971, 2009. doi:10.1016/j.biocel.2009.03.011.
52. **Madrigal-Matute J, Fernandez-Laso V, Sastre C, Llamas-Granda P, Egido J, Martin-Ventura JL, Zalba G, Blanco-Colio LM.** TWEAK/Fn14 interaction promotes oxidative stress through NADPH oxidase activation in macrophages. *Cardiovasc Res* 108: 139–147, 2015. doi:10.1093/cvr/cvv204.
53. **Mak KM, Png CY, Lee DJ.** Type V collagen in health, disease, and fibrosis. *Anat Rec (Hoboken)* 299: 613–629, 2016. doi:10.1002/ar.23330.
54. **Mandl A, Huong Pham L, Toth K, Zambetti G, Erhardt P.** Puma deletion delays cardiac dysfunction in murine heart failure models through attenuation of apoptosis. *Circulation* 124: 31–39, 2011. doi:10.1161/CIRCULATIONAHA.110.988303.
55. **Mangubat M, Lutfy K, Lee ML, Pulido L, Stout D, Davis R, Shin CS, Shahbazian M, Seasholtz S, Sinha-Hikim A, Sinha-Hikim I, O'Dell LE, Lyzlov A, Liu Y, Friedman TC.** Effect of nicotine on body composition in mice. *J Endocrinol* 212: 317–326, 2012. doi:10.1530/JOE-11-0350.
56. **Miedema MD, Maziarz M, Biggs ML, Zieman SJ, Kizer JR, Ix JH, Mozaffarian D, Tracy RP, Psaty BM, Siscovick DS, Mukamal KJ, Djousse L.** Plasma-free fatty acids, fatty acid-binding protein 4, and mortality in older adults (from the Cardiovascular Health Study). *Am J Cardiol* 114: 843–848, 2014. doi:10.1016/j.amjcard.2014.06.012.
57. **Mitchell T, Johnson MS, Ouyang X, Chacko BK, Mitra K, Lei X, Gai Y, Moore DR, Barnes S, Zhang J, Koizumi A, Ramanadham S, Darley-Usmar VM.** Dysfunctional mitochondrial bioenergetics and oxidative stress in Akita(+/Ins2)-derived β-cells. *Am J Physiol Endocrinol Metab* 305: E585–E599, 2013. doi:10.1152/ajpendo.00093.2013.
58. **Miyazaki M, Esser KA.** REDD2 is enriched in skeletal muscle and inhibits mTOR signaling in response to leucine and stretch. *Am J Physiol Cell Physiol* 296: C583–C592, 2009. doi:10.1152/ajpcell.00464.2008.
59. **Morton LF, Barnes MJ.** Collagen polymorphism in the normal and diseased blood vessel wall. Investigation of collagens types I, III and V. *Atherosclerosis* 42: 41–51, 1982. doi:10.1016/0021-9150(82)90124-1.
60. **Nelluri B, Murphy K, Mookadam F, Mookadam M.** The current literature regarding the cardiovascular effects of electronic cigarettes. *Future Cardiol* 12: 167–179, 2016. doi:10.2217/fca.15.83.
61. **Nojiri H, Shimizu T, Funakoshi M, Yamaguchi O, Zhou H, Kawakami S, Ohta Y, Sami M, Tachibana T, Ishikawa H, Kurosawa H, Kahn RC, Otsu K, Shirasawa T.** Oxidative stress causes heart failure with impaired mitochondrial respiration. *J Biol Chem* 281: 33789–33801, 2006. doi:10.1074/jbc.M602118200.
62. **OECD.** Guidance Document on Acute Inhalation Toxicity Testing Vol. Series on Testing and Assessment. *Series on Testing and Assesment* 39: 1–71, 2009.
63. **Olfert IM, DeVallance E, Hoskinson H, Branyan KW, Clayton S, Pitzer CR, Sullivan DP, Breit MJ, Wu ZX, Klinkhachorn P, Mandler WK, Erdreich BH, Ducatman BS, Bryner RW, Dasgupta P, Chantler PD.** Chronic exposure to electronic cigarette (E-cig) results in impaired cardiovascular function in mice. *J Appl Physiol* 124: 573–582, 2018. doi:10.1152/japplphysiol.00713.2017.
64. **Patenge N.** Quantification of DNA damage and repair in mitochondrial, nuclear, and bacterial genomes by real-time PCR. *Methods Mol Biol* 1644: 159–166, 2017. doi:10.1007/978-1-4939-7187-9_14.
65. **Pendse AA, Arbones-Mainar JM, Johnson LA, Altenburg MK, Maeda N.** Apolipoprotein E knock-out and knock-in mice: atherosclerosis, metabolic syndrome, and beyond. *J Lipid Res* 50, *Suppl*: S178–S182, 2009. doi:10.1194/jlr.R800070-JLR200.
66. **Rapti K, Diokmetzidou A, Kloukina I, Milner DJ, Varela A, Davos CH, Capetanaki Y.** Opposite effects of catalase and MnSOD ectopic expression on stress induced defects and mortality in the desmin deficient cardiomyopathy model. *Free Radic Biol Med* 110: 206–218, 2017. doi:10.1016/j.freeradbiomed.2017.06.010.
67. **Redmann M, Benavides GA, Wani WY, Berryhill TF, Ouyang X, Johnson MS, Ravi S, Mitra K, Barnes S, Darley-Usmar VM, Zhang J.** Methods for assessing mitochondrial quality control mechanisms and cellular consequences in cell culture. *Redox Biol* 17: 59–69, 2018. doi:10.1016/j.redox.2018.04.005.
68. **Ren MY, Sui SJ.** The role of TWEAK/Fn14 in cardiac remodeling. *Mol Biol Rep* 39: 9971–9977, 2012. doi:10.1007/s11033-012-1867-6.
69. **Robinson MD, McCarthy DJ, Smyth GK.** edgeR: a Bioconductor package for differential expression analysis of digital gene expression data. *Bioinformatics* 26: 139–140, 2010. doi:10.1093/bioinformatics/btp616.
70. **Roos KP, Jordan MC, Fishbein MC, Ritter MR, Friedlander M, Chang HC, Rahgozar P, Han T, Garcia AJ, Maclellan WR, Ross RS, Philipson KD.** Hypertrophy and heart failure in mice overexpressing the cardiac sodium-calcium exchanger. *J Card Fail* 13: 318–329, 2007. doi:10.1016/j.cardfail.2007.01.004.
71. **Schönfeld P, Wojtczak L.** Fatty acids as modulators of the cellular production of reactive oxygen species. *Free Radic Biol Med* 45: 231–241, 2008. doi:10.1016/j.freeradbiomed.2008.04.029.
72. **Schroeder AM, Wang HB, Park S, Jordan MC, Gao F, Coppola G, Fishbein MC, Roos KP, Ghiani CA, Colwell CS.** Cardiac dysfunction in the BACHD mouse model of Huntington's disease. *PLoS One* 11: e0147269, 2016. doi:10.1371/journal.pone.0147269.
73. **Shao XM, Liu S, Lee ES, Fung D, Pei H, Liang J, Mudgway R, Zhang J, Feldman JL, Zhu Y, Louie S, Xie XS.** Chronic intermittent nicotine delivery via lung alveolar region-targeted aerosol technology produces circadian pharmacokinetics in rats resembling human smokers. *J Appl Physiol (1985)* 125: 1555–1562, 2018. doi:10.1152/japplphysiol.00357.2018.
74. **Shao XM, Xu B, Liang J, Xie XS, Zhu Y, Feldman JL.** Nicotine delivery to rats via lung alveolar region-targeted aerosol technology produces blood pharmacokinetics resembling human smoking. *Nicotine Tob Res* 15: 1248–1258, 2013. doi:10.1093/ntr/nts261.
75. **Sinha-Hikim I, Friedman TC, Falz M, Chalfant V, Hasan MK, Espinoza-Derout J, Lee DL, Sims C, Tran P, Mahata SK, Sinha-Hikim AP.** Nicotine plus a high-fat diet triggers cardiomyocyte apoptosis. *Cell Tissue Res* 368: 159–170, 2017. doi:10.1007/s00441-016-2536-1.
76. **Sinha-Hikim I, Friedman TC, Shin CS, Lee D, Ivey R, Sinha-Hikim AP.** Nicotine in combination with a high-fat diet causes intramyocellular mitochondrial abnormalities in male mice. *Endocrinology* 155: 865–872, 2014. doi:10.1210/en.2013-1795.

77. **Swirski FK, Nahrendorf M.** Leukocyte behavior in atherosclerosis, myocardial infarction, and heart failure. *Science* 339: 161–166, 2013. doi:10.1126/science.1230719.
78. **Trtchounian A, Williams M, Talbot P.** Conventional and electronic cigarettes (e-cigarettes) have different smoking characteristics. *Nicotine Tob Res* 12: 905–912, 2010. doi:10.1093/ntr/ntq114.
79. **USEPA.** *Health Effects Test Guidelines OPPTS 870.1300 Acute Inhalation Toxicity*. Washington, DC: Environmental Protection Agency, Prevention, Pesticides, and Toxic Substance, 1998.
80. **Wang C, Chen H, Zhu W, Xu Y, Liu M, Zhu L, Yang F, Zhang L, Liu X, Zhong Z, Zhao J, Jiang J, Xiang M, Yu H, Hu X, Lu H, Wang J.** Nicotine accelerates atherosclerosis in apolipoprotein E-deficient mice by activating α7 nicotinic acetylcholine receptor on mast cells. *Arterioscler Thromb Vasc Biol* 37: 53–65, 2017. doi:10.1161/ATVBAHA.116.307264.
81. **Wang Z, Wang D, Wang Y.** Cigarette smoking and adipose tissue: the emerging role in progression of atherosclerosis. *Mediators Inflamm* 2017: 1–11, 2017. doi:10.1155/2017/3102737.
82. **Wu Y, Song P, Zhang W, Liu J, Dai X, Liu Z, Lu Q, Ouyang C, Xie Z, Zhao Z, Zhuo X, Viollet B, Foretz M, Wu J, Yuan Z, Zou MH.** Activation of AMPKα2 in adipocytes is essential for nicotine-induced insulin resistance in vivo. *Nat Med* 21: 373–382, 2015. doi:10.1038/nm.3826.
83. **Young ME, Wilson CR, Razeghi P, Guthrie PH, Taegtmeyer H.** Alterations of the circadian clock in the heart by streptozotocin-induced diabetes. *J Mol Cell Cardiol* 34: 223–231, 2002. doi:10.1006/jmcc.2001.1504.
84. **Zaragoza C, Gomez-Guerrero C, Martin-Ventura JL, Blanco-Colio L, Lavin B, Mallavia B, Tarin C, Mas S, Ortiz A, Egido J.** Animal models of cardiovascular diseases. *J Biomed Biotechnol* 2011: 1–13, 2011. doi:10.1155/2011/497841.